



OPEN A novel sodium Iron silicate composite with chitosan for efficient removal of Cd(II) ions from water

Mohamed S. Kamel^{1✉}, Ehab A. Abdelrahman^{2✉}, Zinab M. Anwar¹, Samir M. El Rayes¹, Mortaga M. Abou-Krishna², Raed M. Hegazy³ & Hanan Alhussain²

Cadmium ions constitute a major threat to human health and the environment owing to their toxicity, bioaccumulation, and persistence in water bodies, causing renal dysfunction, cancer, and cardiovascular diseases. Hence, this study reports the facile fabrication of a novel sodium iron oxide silicate@amorphous sodium iron silicate product (S1) and its chitosan composite (S1@chitosan) for the high-performance separation of Cd(II) ions from aquatic environments. The Brunauer-Emmett-Teller surface area, total pore volume, and mean pore diameter of S1 were 94.97 m²/g, 0.5853 cm³/g, and 25.65 nm, respectively, while those for S1@chitosan were 30.94 m²/g, 0.09518 cm³/g, and 12.31 nm, respectively. The reduction in pore diameter, pore volume, and surface area confirms the successful functionalization of S1 with chitosan, as the chitosan coating partially blocks and fills the pores, reducing the available surface area and porosity. Also, scanning electron microscope (SEM) images revealed an uneven surface morphology for S1 and a more textured and rougher surface for S1@chitosan, supporting the incorporation of chitosan. Besides, energy-dispersive X-ray spectroscopy (EDX) and CHN analyses affirmed the existence of chitosan in the composite through the detection of carbon and nitrogen elements, characteristic of chitosan. The optimum conditions for the removal of Cd(II) ions were determined to be a contact time of 70 min for S1 and 50 min for S1@chitosan, a pH of 7.50, and a temperature of 298 K. The maximum sorption capacities were 284.09 mg/g for S1 and 389.11 mg/g for S1@chitosan. The removal mechanism for S1 primarily involves ion exchange, while S1@chitosan utilizes both ion exchange and complexation through the amino and hydroxyl groups of chitosan. Regeneration using HCl confirmed the effective reusability of both adsorbents over five successive cycles. The adsorption process was found to be chemical, exothermic, and best described by the pseudo-second-order kinetic model and Langmuir isotherm.

Keywords Adsorption efficiency, Cd(II) ions, Sodium iron oxide silicate@amorphous sodium iron silicate, Chitosan functionalization, Regeneration and reusability

Heavy metals from industrial, urban, and agricultural activities contaminate water and cause serious environmental and health risks^{1–6}. In humans, they are linked to neurological issues, organ damage, cardiovascular diseases, and cancer^{7–10}. Cd(II) ions are highly toxic, persist in the body, and can cause organ damage, osteoporosis, cancer, and cardiovascular diseases by disrupting calcium metabolism^{11–14}. Various methods have been employed to remove heavy metals from contaminated water, including chemical precipitation¹⁵, membrane filtration¹⁶, electrochemical¹⁷, and adsorption¹⁸. Among these, adsorption has gained significant attention owing to its simplicity, cost-effectiveness, high efficiency, and the possibility of utilizing a wide range of adsorbent materials. Adsorption is a process that includes the adhesion of heavy metal ions onto the surface of solid materials, which can then be separated from the water. It is considered a versatile method that can be applied to treat water contaminated with low concentrations of heavy metals, making it suitable for various water treatment scenarios¹⁹. The adsorption method offers several advantages over other techniques for removing heavy metals. Unlike chemical precipitation, adsorption does not require large quantities of chemicals, making it an environmentally

¹Chemistry Department, Faculty of Science, Suez Canal University, Ismailia 41522, Egypt. ²Department of Chemistry, College of Science, Imam Mohammad Ibn Saud Islamic University (IMSIU), 11623 Riyadh, Saudi Arabia.

³Egyptian Petroleum Research Institute, Ahmed El Zumer Street, Nasr City, Hai Al-Zehour, Cairo 11727, Egypt. ✉email: mohamedkamel18880@gmail.com; EAAAhmed@imamu.edu.sa

friendly process. Compared to membrane filtration and electrochemical methods, adsorption is less energy-intensive and can be conducted using simple equipment, making it accessible to regions with limited resources. Adsorbents used in this process can often be regenerated and reused, enhancing the sustainability of the method. Additionally, adsorption can achieve high removal efficiencies, even at low concentrations of heavy metals, due to the high affinity of certain adsorbent materials for metal ions²⁰. Lately, there has been a surge in interest regarding the application of metal oxides, amorphous sodium aluminum silicates, and chitosan composites for the adsorption of heavy metals. Metal oxides, such as iron-manganese oxide and cobalt ferrite, possess high surface areas and active sites, making them effective adsorbents for heavy metal ions^{21–23}. Amorphous sodium aluminum silicates, with their high surface area, porosity, and high adsorption capacity due to the sodium ion-exchange property, provide excellent adsorption capacities and selectivity for various heavy metals^{24,25}. Chitosan, a biopolymer derived from chitin, has been extensively explored for its adsorption properties. Various composites, including carbon nanotubes/chitosan²⁶, boehmite/chitosan²⁷, chitosan/Fe₃O₄/bentonite²⁸, magnetic graphene oxide/chitosan²⁹, and vermiculite/chitosan³⁰, have been developed to enhance metal ion removal efficiency due to the presence of amino and hydroxyl functional groups that can form complexes with metal ions. Composites of these materials combine the advantages of their individual components, resulting in synergistic effects that enhance adsorption performance, stability, and reusability. The current research introduces an innovative aspect by synthesizing a novel sodium iron oxide silicate@amorphous sodium iron silicate product and its chitosan composite for the high-performance separation of Cd(II) ions from aquatic environments. The design of this new composite combines the ion-exchange adsorption property of sodium iron oxide silicate@amorphous sodium iron silicate product with the adsorption complexation property of chitosan functional groups (NH₂ and OH), resulting in a unique adsorbent with enhanced properties. The composite's ability to effectively adsorb and remove Cd(II) ions from aqueous media is examined under various experimental conditions, including different pH levels, contact times, temperatures, and preliminary concentrations of Cd(II). Additionally, the regeneration efficiency and reusability of the adsorbents were systematically evaluated.

Experimental Chemicals

Iron(III) chloride hexahydrate (FeCl₃·6H₂O), sodium hydroxide (NaOH), sodium metasilicate pentahydrate (Na₂SiO₃·5H₂O), cadmium(II) nitrate tetrahydrate (Cd(NO₃)₂·4H₂O), chitosan ((C₆H₁₁NO₄)_n), and hydrochloric acid (HCl) were obtained from Sigma-Aldrich chemical company.

Synthesis of adsorbents

Synthesis of sodium iron oxide silicate@amorphous sodium iron silicate

To synthesize sodium iron oxide silicate@amorphous sodium iron silicate, 15.00 g sodium metasilicate pentahydrate (Na₂SiO₃·5H₂O) was solubilized in 70 mL distilled water. Separately, 4.00 g iron(III) chloride hexahydrate (FeCl₃·6H₂O) was solubilized in another 70 mL distilled water. A solution of FeCl₃·6H₂O was gradually added dropwise to the Na₂SiO₃·5H₂O solution under continuous stirring for 60 min. The resulting precipitate was separated by filtration, thoroughly washed with distilled water multiple times to remove any residual impurities, and dried at room temperature to obtain the desired sodium iron oxide silicate@amorphous sodium iron silicate. Figure 1A illustrates the synthesis process of sodium iron oxide silicate@amorphous sodium iron silicate, which was abbreviated as S1.

Synthesis of S1@chitosan composite

To synthesize the S1@chitosan composite, 2.00 g chitosan was dissolved in 120 mL of a 1 M acetic acid solution. After that, 2.00 g of the S1 sample was added to the chitosan solution with stirring continuously for 2 h. The mixture obtained in the previous step was then incorporated into 250 mL of a 0.50 M NaOH solution with stirring continuously for another 2 h to facilitate the formation of the composite. The resulting product was filtered, thoroughly washed with distilled water to remove any residual impurities, and dried at room temperature to obtain the S1@chitosan composite. Figure 1B illustrates the synthesis process of the S1@chitosan composite.

Instrumentation

The structural properties of the S1 and S1@chitosan samples were analyzed using an X-ray diffraction (XRD) system (X'Pert PRO, PANalytical, Netherlands) to determine their crystalline phases. The porosity and specific surface area of the samples were measured utilizing a surface area analyzer (NOVA2000 series, Quantachrome, USA). A scanning electron microscope (SEM) (JSM-6510LV, JEOL Ltd., Japan) was employed to observe the surface morphology, while elemental composition was assessed using energy-dispersive X-ray spectroscopy (EDX) (X-Max 20, Oxford, England). The elemental composition of carbon, hydrogen, and nitrogen in the S1@chitosan sample was determined using a CHN Elemental Analyzer (PerkinElmer, 2400 Series II, USA).

Removal of Cd(II) ions from aqueous media

The removal of Cd(II) ions from aqueous media was performed under various experimental conditions to investigate the effects of pH, contact time, temperature, and initial concentration on the adsorption efficiency using S1 and S1@chitosan adsorbents. The experimental conditions for these studies are summarized in Table 1. After the stirring process is completed, the adsorbent is separated from the solution by centrifugation, and the final concentration of Cd(II) ions remaining in the resulting filtrate is accurately measured utilizing an atomic absorption spectrophotometer (AAS ZEE nit 700 p, Analytik Jena AG, Germany).

Besides, the separation percentage of Cd(II) ions (% R) as well as sorption capacity of the synthesized adsorbents (Q) were calculated utilizing Eqs. (1) and (2), respectively^{31,32}.

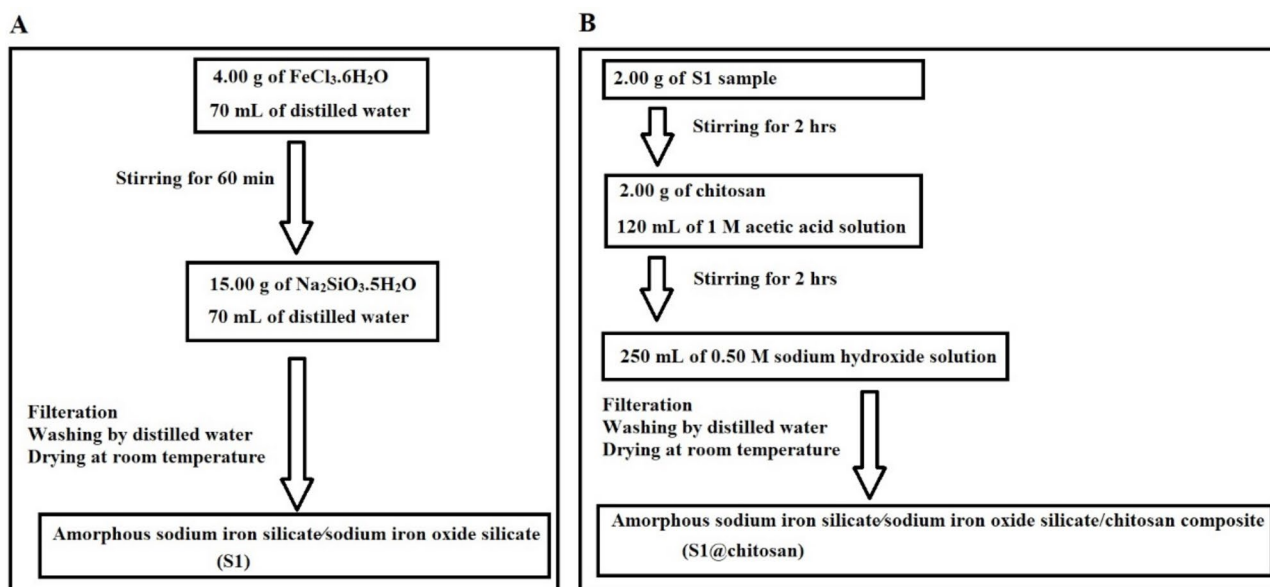


Fig. 1. Schematic representation of the synthesis processes of (A) S1 and (B) S1@chitosan adsorbents.

Effect	pH	Time (min)	Temperature (K)	Concentration (mg/L)
Cd(II) solution volume (mL)	100	100	100	100
Cd(II) solution concentration (mg/L)	200	200	200	50–300
Temperature (K)	298	298	298–328	298
Stirring time (min)	180	10–100	70 (S1) 50 (S1@chitosan)	70 (S1) 50 (S1@chitosan)
Quantity of adsorbent	0.05	0.05	0.05	0.05
pH	2.5–7.5	7.5	7.5	7.5

Table 1. Experimental conditions for investigating the effect of pH, time, temperature, and concentration on the adsorption efficiency of Cd(II) ions using S1 and S1@chitosan adsorbents.

$$\% R = \frac{C_o - C_e}{C_o} \times 100 \quad (1)$$

$$Q = (C_o - C_e) \times \frac{V}{W} \quad (2)$$

where, C_o describes the preliminary concentration of Cd(II) ions (mg/L) and C_e describes the concentration of Cd(II) ions at equilibrium state (mg/L). Also, V describes the total volume of the Cd(II)-containing solution (L) and W describes the mass of the adsorbent (g).

The regeneration of Cd(II)-laden adsorbent was conducted to evaluate the desorption efficiency of Cd(II) ions using hydrochloric acid (HCl) as the eluting agent. Three different concentrations of HCl (0.5 M, 1 M, and 1.5 M) were prepared, and 50 mL of each solution was used for the desorption process. The adsorbent containing Cd(II) ions was treated with the respective eluting agent solutions then stirred for 30 min to release the adsorbed Cd(II) ions. Using Eq. 3, the desorption percentage of Cd(II) ions (% D) was evaluated³³.

$$\% D = \frac{100C_dV_d}{(C_o - C_e)V} \quad (3)$$

where, C_d describes the concentration of Cd(II) ions in the desorbing solution (mg/L) whereas V_d describes the volume of the desorbing solution (L).

The reusability of S1 and S1@chitosan adsorbents for the separation of Cd(II) ions was evaluated over five consecutive adsorption-desorption cycles using Eq. (1). Each cycle was performed using a Cd(II) solution with an initial concentration of 200 mg/L and a volume of 100 mL. The amount of adsorbent used in each cycle was 0.05 g. The experiments were conducted at a temperature of 298 K and a pH of 7.5. The contact time for each cycle was 70 min for S1 and 50 min for S1@chitosan.

Results and discussion

Characterization of S1 and S1@chitosan composite

The XRD analysis of the S1 sample, which is a crystalline sodium iron oxide silicate@amorphous sodium iron silicate, reveals a broad band characteristic of amorphous sodium iron silicate at 2θ angle equals 31.12° , as shown in Fig. 2. For the crystalline sodium iron oxide silicate phase, distinct peaks were observed at the following 2θ angles: 29.09° , 31.49° , 32.49° , 33.79° , 40.03° , 43.85° , 49.12° , 52.97° , and 57.74° . These peaks correspond to the miller indices (123), (114), (132), (124), (142), (135), (008), (062), and (245), respectively. In contrast, the S1@

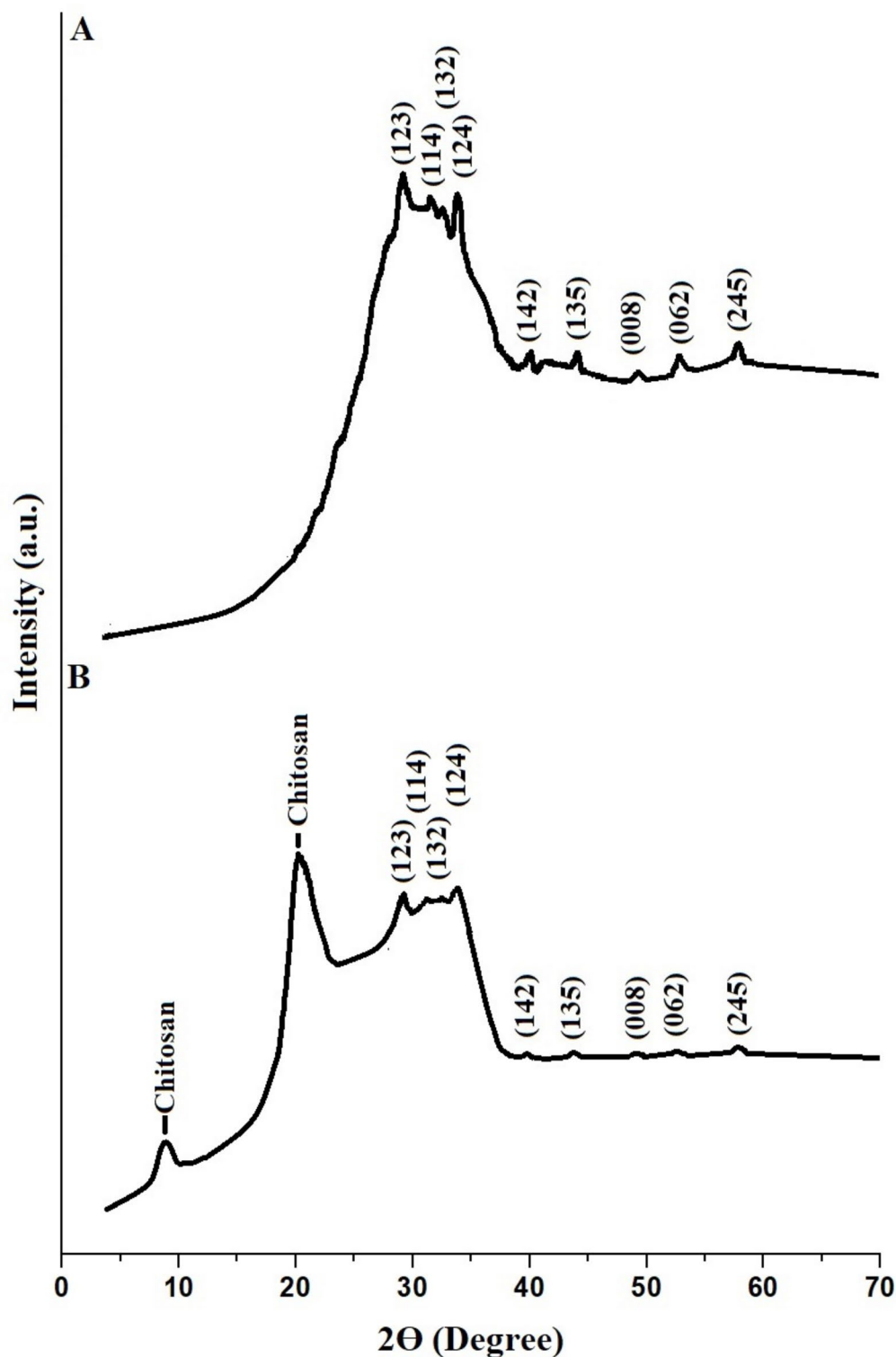


Fig. 2. XRD of (A) S1 and (B) S1@chitosan samples.

chitosan sample, which is an amorphous sodium iron silicate/sodium iron oxide silicate/chitosan composite, shows characteristic peaks of chitosan at 2θ angles of 8.90° and 20.28° , in addition to the peaks observed for the S1 sample, indicating the successful incorporation of chitosan into the composite structure. The decrease observed in the intensity of the characteristic peaks of sodium iron oxide silicate in the S1@chitosan sample compared to the S1 sample is attributed to the incorporation of chitosan. The incorporation of chitosan into the composite structure leads to a reduction in the crystallinity of the sodium iron oxide silicate phase, as chitosan is an amorphous material that can obscure the diffraction signals of the crystalline phases. This reduction in peak intensity confirms the successful integration of chitosan within the composite, thereby altering its structural properties.

The FTIR spectrum of S1 (sodium iron oxide silicate@amorphous sodium iron silicate) product, as shown in Fig. 3A, exhibits distinct vibrational bands confirming the presence of key functional groups. A broad band observed at 3207 cm^{-1} is attributed to O–H stretching vibrations, indicating hydroxyl groups and adsorbed water molecules. A peak at 1601 cm^{-1} corresponds to H–O–H bending vibrations, suggesting the presence of water molecules or hydrated components. A strong absorption around 982 cm^{-1} is assigned to Si–O–Si and Si–O–Fe stretching vibrations, confirming the silicate framework and its interaction with iron oxide. A characteristic peak at 642 cm^{-1} represents Fe–O stretching vibrations supporting the formation of iron oxide phases. Sharp bands at 473 cm^{-1} correspond to Fe–O and Fe–O–Si vibrational modes, further validating the interaction between iron oxide and the silicate matrix. The FTIR spectrum of S1@Chitosan composite (Fig. 3B) exhibits distinct vibrational bands that confirm the presence of key functional groups from both S1 and chitosan components. The band at 1153 cm^{-1} is due to C–O–C stretching vibrations from chitosan, indicating the presence of ether linkages in the polymer backbone. The peak at 1601 cm^{-1} corresponds to H–O–H bending vibrations, suggesting the presence of water molecules or amide functional groups from chitosan. The band at 2900 cm^{-1} arises from C–H stretching vibrations, confirming the presence of aliphatic bonds in chitosan. The broad band at 3440 cm^{-1} is attributed to O–H and N–H stretching vibrations, confirming the presence of hydroxyl and amine functional groups from chitosan and possible hydrogen bonding within the composite.

The energy-dispersive X-ray spectroscopy (EDX) analysis described in Fig. 4A,B demonstrates the elemental composition of the S1 and S1@chitosan samples, respectively. The EDX spectra show significant changes in the elemental composition upon functionalization of the S1 sample with chitosan, as summarized in Table 2. In the EDX spectrum of S1 (Fig. 4A), the dominant elements observed are oxygen (O), sodium (Na), silicon (Si), and iron (Fe). The atomic percentages of O (48.48%), Na (15.79%), Si (24.54%), and Fe (11.19%) further corroborate the composition of the S1 sample as primarily consisting of these elements. In contrast, the EDX spectrum of the S1@chitosan sample (Fig. 4B) reveals additional peaks corresponding to carbon (C) and nitrogen (N), which are characteristic of the chitosan polymer. The appearance of C (24.30%) and N (18.11%) signals, along with a noticeable decrease in the atomic percentages of O (37.27%), Na (7.06%), Si (7.61%), and Fe (5.65%), indicates successful functionalization of the S1 sample with chitosan. Besides, The CHN elemental analysis of the S1@chitosan sample provides further confirmation of the successful functionalization of the S1 sample with chitosan. The analysis shows a carbon (C) content of 20.08%, a hydrogen (H) content of 1.45%, and a nitrogen (N) content of 9.92%, which are characteristic of the chitosan structure. Chitosan is a polysaccharide rich in carbon, hydrogen, and nitrogen due to its repeating glucosamine units containing amino ($-\text{NH}_2$) groups. The presence of significant amounts of carbon and nitrogen in the S1@chitosan sample is consistent with the incorporation of chitosan onto the surface of S1 sample. The observed nitrogen content (9.92%) in particular is a strong indicator of chitosan presence since nitrogen is not naturally found in the original S1 sample. This is further supported by the notable carbon content (20.08%), which aligns with the carbon-rich nature of the chitosan polymer. The relatively low hydrogen content (1.45%) can be explained by the fact that while chitosan contains hydrogen, its contribution to the total weight% is less pronounced compared to carbon and nitrogen due to the molecular structure of chitosan and the composition of S1. The data from the CHN analysis corroborates the elemental results from the EDX analysis, which also showed an increase in carbon and nitrogen percentages after the functionalization of S1 with chitosan.

Figure 5 shows the nitrogen adsorption-desorption isotherms for the S1 and S1@chitosan samples, illustrating their surface properties across a range of relative pressures. The isotherms reveal a significant difference in the adsorption behavior between the two samples, indicating that S1 has a higher adsorption capacity compared to S1@chitosan. Table 3 provides quantitative data on the BET surface area, mean pore diameter, as well as total pore volume for both samples. The BET surface area of S1 is $94.97\text{ m}^2/\text{g}$, while that of S1@chitosan is reduced to $30.94\text{ m}^2/\text{g}$. Similarly, the mean pore diameter and total pore volume of the S1 sample are larger, with values of 25.65 nm and $0.5853\text{ cm}^3/\text{g}$, respectively, compared to 12.31 nm and $0.09518\text{ cm}^3/\text{g}$ for the S1@chitosan sample. The smaller mean pore diameter, total pore volume, and BET surface area of the S1@chitosan sample compared to the S1 sample are likely due to the chitosan incorporation, which blocks some of the pores and reduces the overall porosity in addition to the surface area available for nitrogen adsorption. The reduction in pore size and volume suggests that the chitosan layer fills or partially obstructs the existing pores of the S1 material, thereby limiting the accessible surface area for gas adsorption. The nitrogen adsorption-desorption isotherms of both samples exhibit a type IV isotherm pattern, which is characteristic of mesoporous materials³⁴. The data indicates that both S1 and S1@chitosan samples contain mesopores since their average pore sizes are greater than 2 nm , aligning with the IUPAC definition of mesoporous materials.

Figure 6A,B shows the SEM images of S1 and S1@chitosan samples, respectively, providing insight into their morphological characteristics before and after functionalization with chitosan. The SEM image of S1 (Fig. 6A) reveals an uneven surface morphology with agglomerated particles, indicative of the amorphous nature of the sodium iron silicate material. The surface appears relatively smooth with scattered aggregates, suggesting a high degree of particle cohesion and some inherent porosity typical of amorphous materials. In contrast, the SEM image of the S1@chitosan sample (Fig. 6B) shows significant changes in the surface morphology upon chitosan

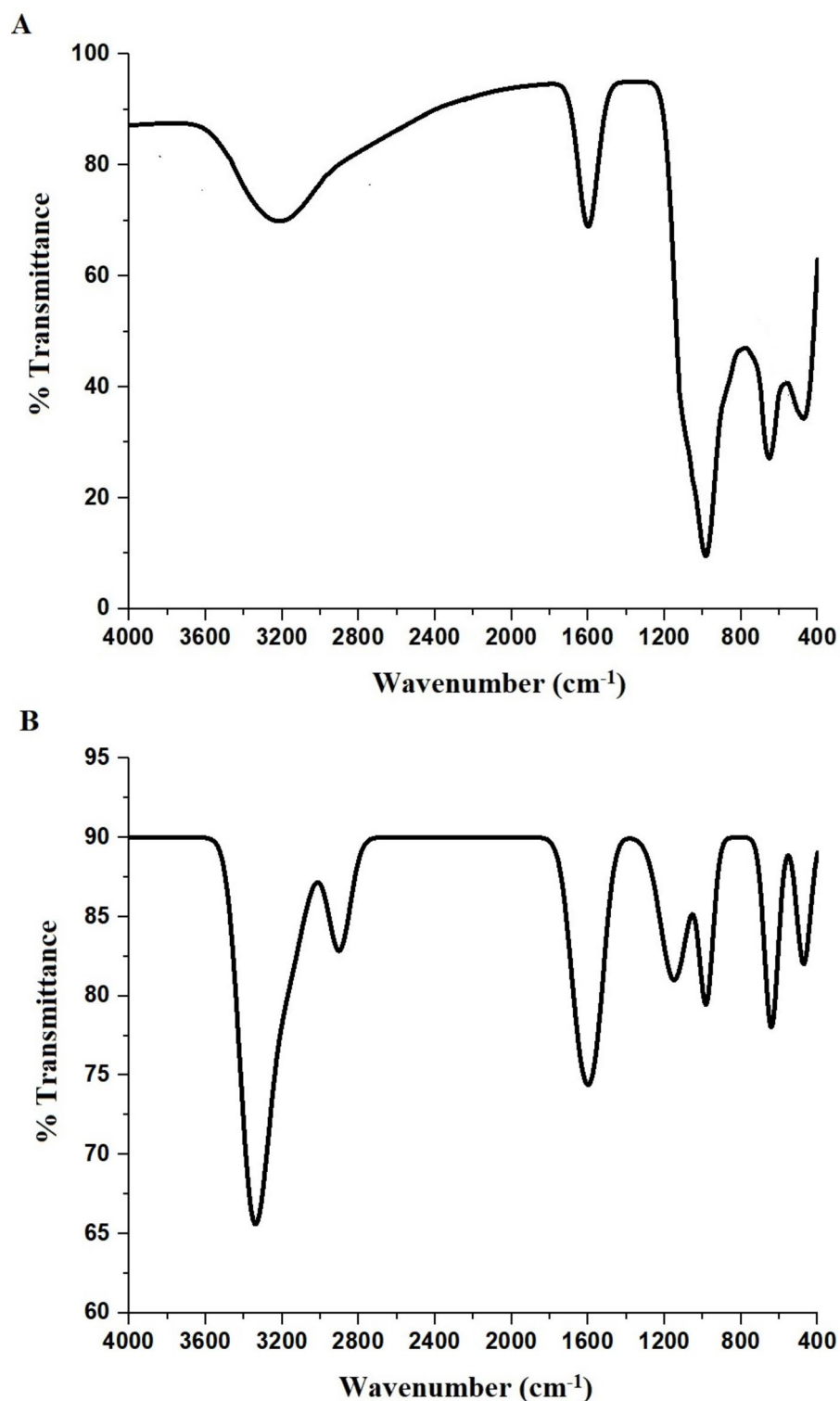


Fig. 3. FTIR of (A) S1 and (B) S1@chitosan samples.

functionalization. The surface of S1@chitosan appears more textured and rougher, with additional layers and flakes covering the material. These changes suggest that the chitosan has successfully functionalized the S1 sample, forming a more complex and interconnected network structure. The increased roughness and the appearance of new morphological features are consistent with the presence of chitosan, which may have penetrated the interstitial spaces between S1 particles, leading to enhanced aggregation and a more heterogeneous surface. The observed morphological transformation from S1 to S1@chitosan, as indicated by the SEM images, supports the successful functionalization of S1 with chitosan.

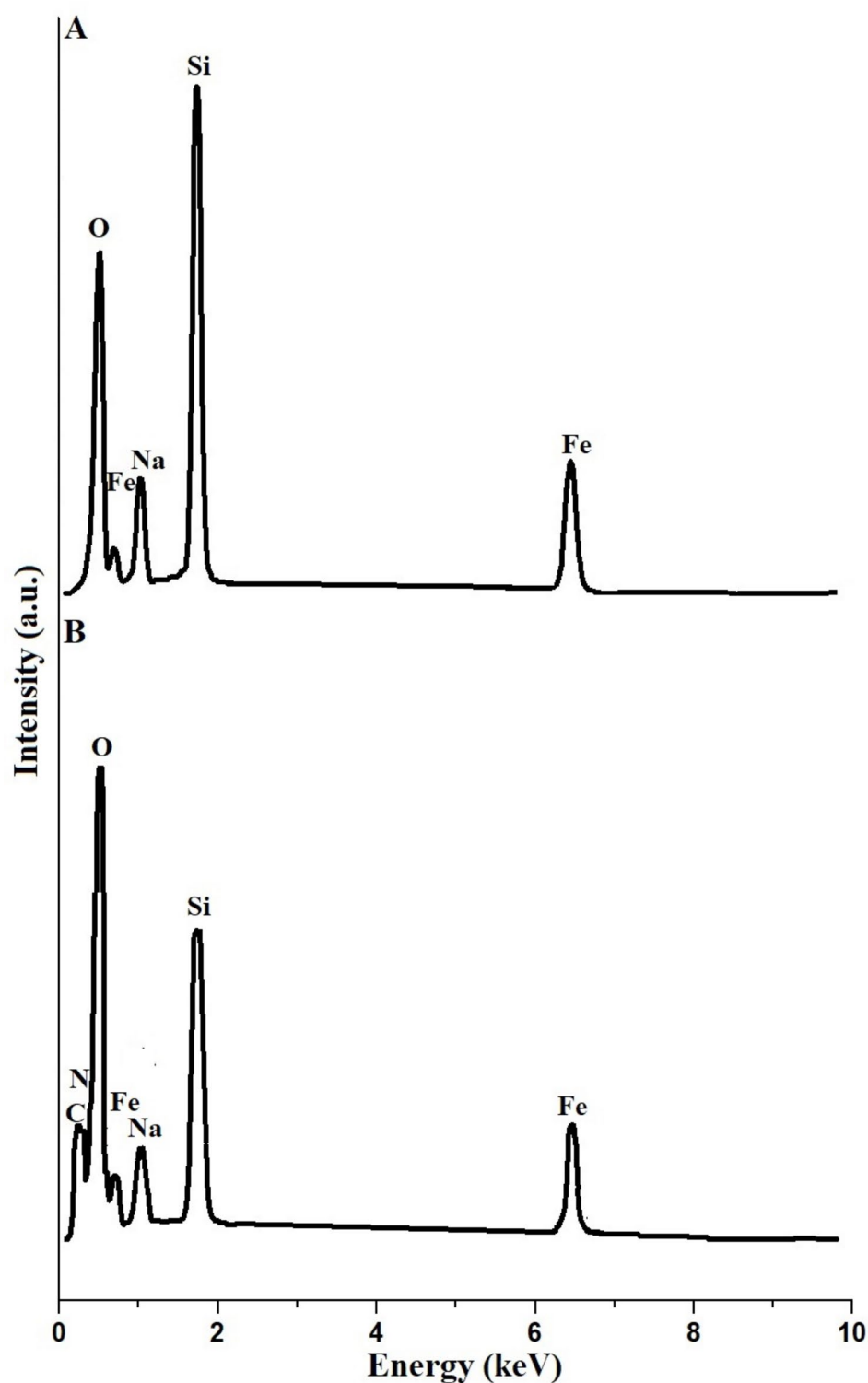


Fig. 4. EDX of (A) S1 and (B) S1@chitosan samples.

Disposal of Cd(II) ions from aqueous environments

Effect of pH

The dependence of the separation efficiency of Cd(II) ions on pH shows that the separation efficiency of Cd(II) ions utilizing the S1 and S1@chitosan adsorbents increases as the pH rises (Fig. 7). At a lower pH of 2.50, the separation efficiency of Cd(II) ions is relatively low, with S1 achieving 2.19% and S1@chitosan achieving 3.44%, indicating minimal adsorption under acidic conditions. This lower separation efficiency at low pH is due to the high concentration of hydrogen ions (H^+) in the solution, which compete with Cd(II) ions for the

Sample	Atomic percentage					
	% O	% Na	% Si	% Fe	% C	% N
S1	48.48	15.79	24.54	11.19	0.00	0.00
S1@chitosan	37.27	7.06	7.61	5.65	24.30	18.11

Table 2. Elemental composition of S1 and S1@chitosan samples.

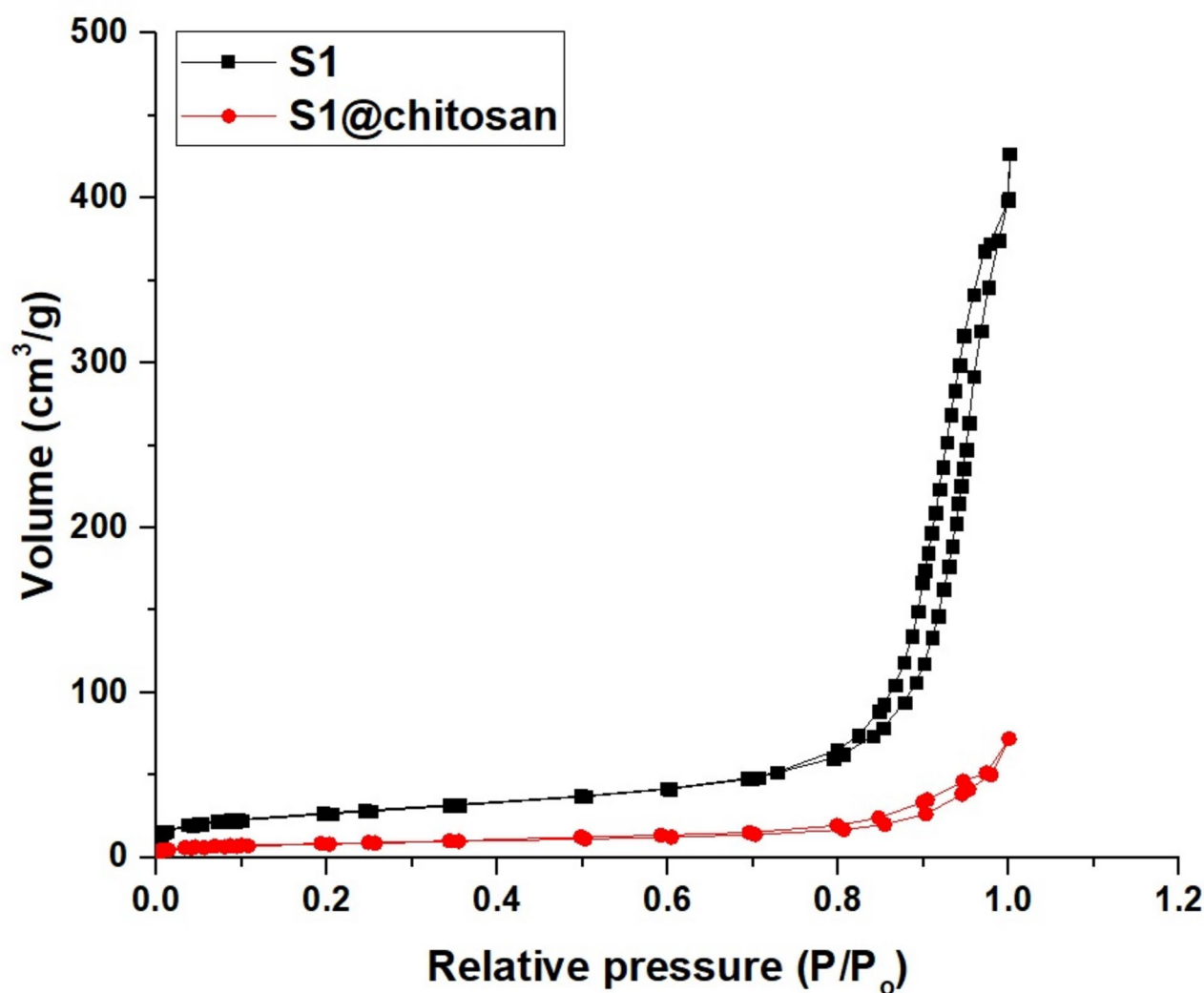


Fig. 5. Nitrogen adsorption-desorption isotherms of S1 and S1@chitosan samples.

Sample	Mean pore diameter (nm)	BET surface area (m²/g)	Total pore volume (cm³/g)
S1	25.65	94.97	0.5853
S1@chitosan	12.31	30.94	0.09518

Table 3. BET surface area, mean pore diameter, and total pore volume characteristics of S1 and S1@chitosan samples.

available adsorption sites on the surface of the adsorbents. Additionally, at reduced pH values, the surface of the adsorbents becomes more protonated, reducing the number of negatively charged sites available for binding with positively charged Cd(II) ions. In contrast, at a higher pH of 7.50, the separation efficiency of Cd(II) ions significantly improves, with S1 reaching 68.40% and S1@chitosan reaching 94.80%. At higher pH values, the

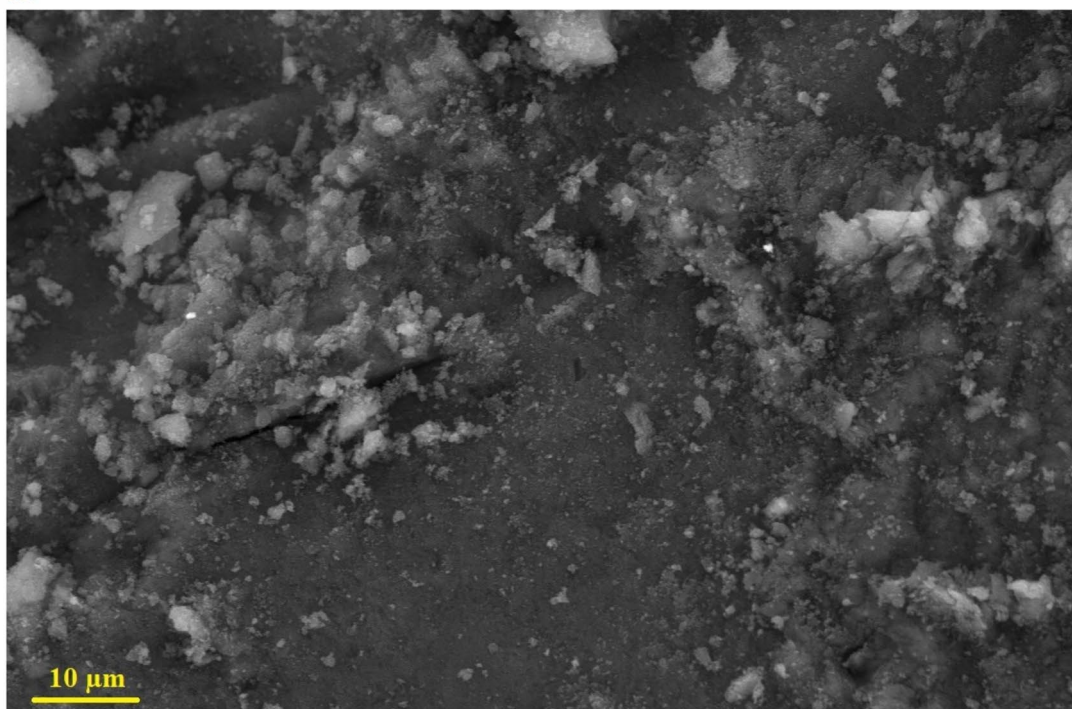
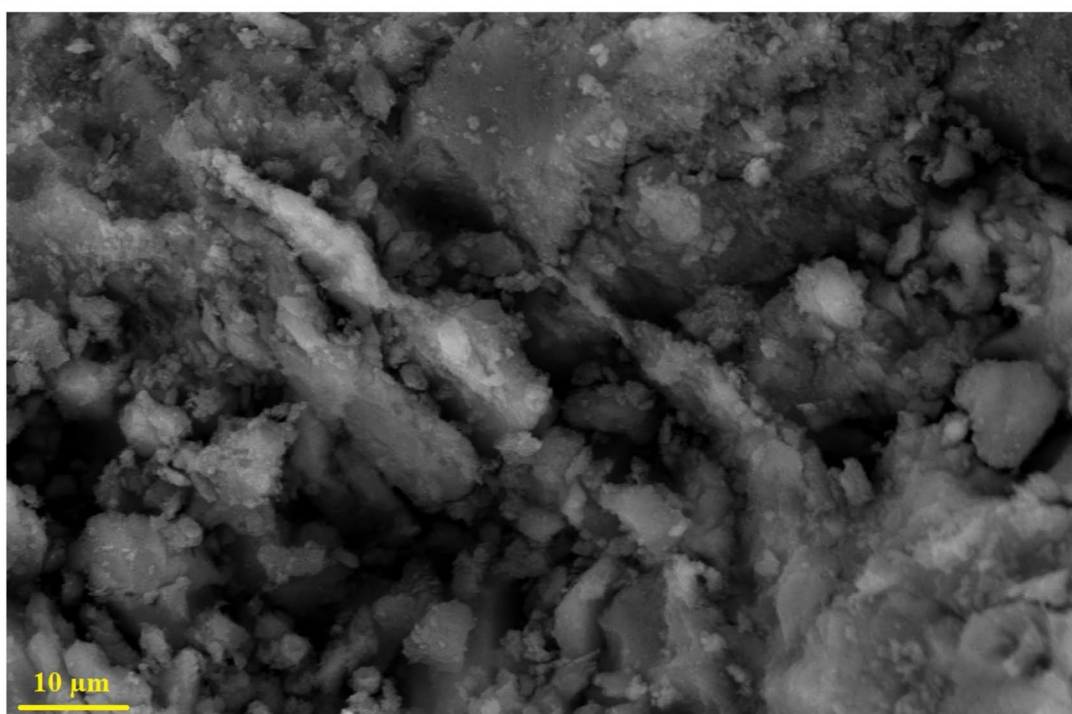
A**B**

Fig. 6. SEM images of (A) S1 and (B) S1@chitosan samples.

concentration of hydrogen ions decreases, reducing competition for adsorption sites and allowing more Cd(II) ions to bind to the adsorbent surface. The S1 adsorbent removes Cd(II) ions primarily through ion exchange, where sodium ions (Na^+) present in the adsorbent are exchanged with Cd(II) ions in the solution. This ion exchange process occurs because, in the S1 adsorbent, some Fe(III) ions substitute certain Si(IV) ions, resulting in a negative charge on the adsorbent's surface. This negative charge is neutralized by Na^+ ions, which are readily exchanged with Cd(II) ions from the solution, enhancing the adsorbent's performance to adsorb Cd(II) ions as the pH increases. The reaction can be expressed by Eq. (4).

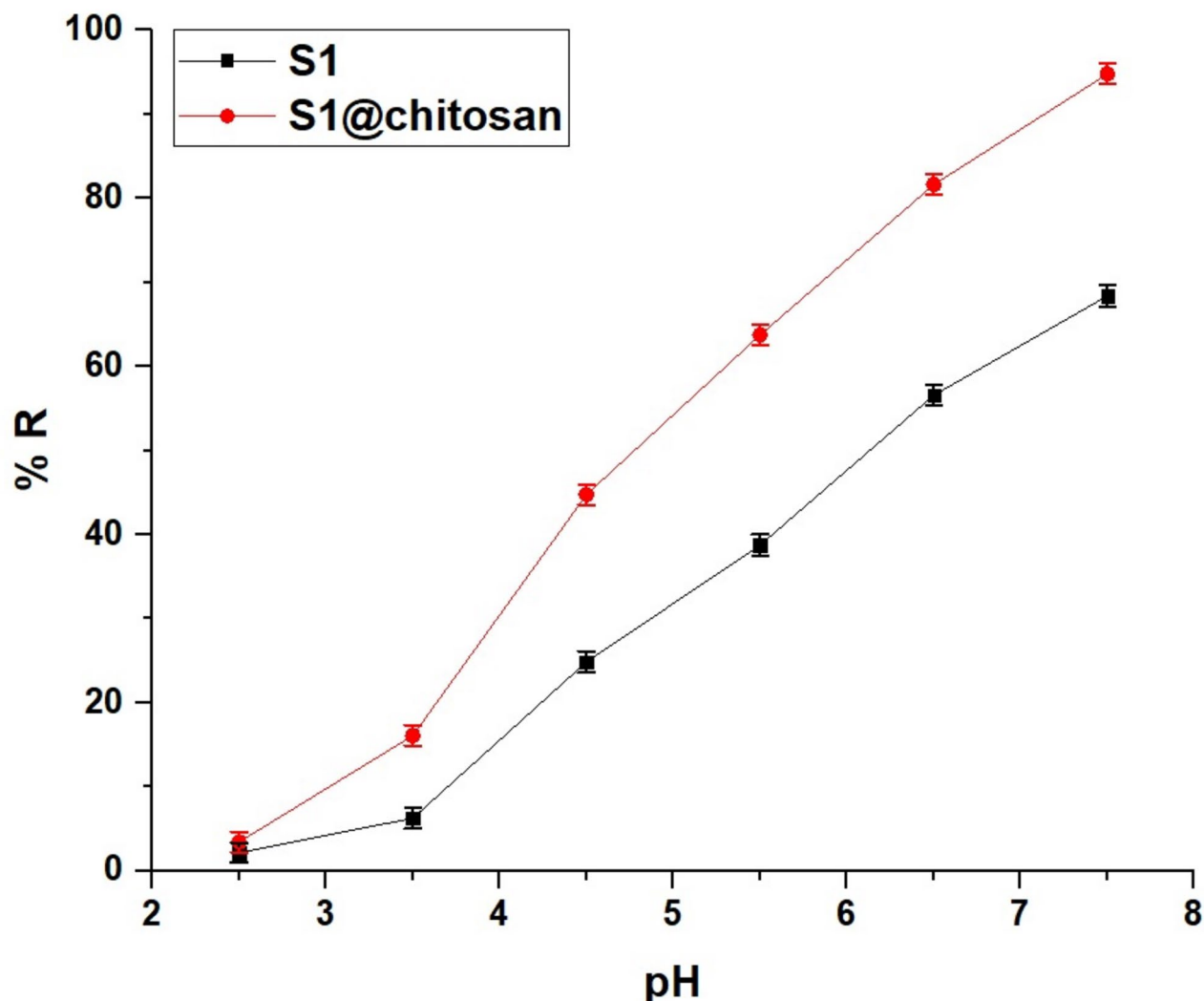
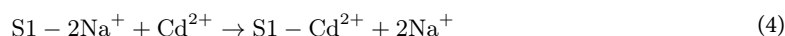
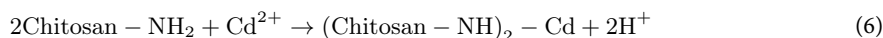
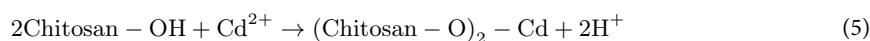


Fig. 7. Effect of solution pH on the separation efficiency of Cd(II) ions utilizing S1 and S1@chitosan samples.



Furthermore, the S1@chitosan adsorbent consistently exhibits a greater removal efficiency compared to S1 due to the combined mechanisms of ion exchange and complexation via the NH_2 and OH groups of chitosan. As the pH rises, the deprotonation of these functional groups occurs, increasing their ability to form complexes with Cd(II) ions, thereby further enhancing the separation efficiency. The complexation process can be represented by Eqs. (5) and (6).



Effect of contact time

The separation efficiency of Cd(II) ions by S1 and S1@chitosan adsorbents increases with time (Fig. 8), reaching an equilibrium point where no further significant change is observed, indicating the saturation of the adsorbent surfaces. For the S1 adsorbent, the removal efficiency equals 34.83% at 10 min and gradually increases to 67.88% at 70 min. Beyond 70 min, the separation efficiency does not change significantly. This indicates that the equilibrium time for the S1 adsorbent is 70 min, beyond which no further adsorption occurs owing to the maximal occupancy of adsorption centers. In contrast, the S1@chitosan adsorbent shows a much faster adsorption process, with the separation efficiency reaching 75.94% at 10 min. The efficiency continues to increase rapidly, reaching 94.38% at 50 min. Beyond 50 min, the separation efficiency remains relatively constant, indicating that the equilibrium time for the S1@chitosan adsorbent is 50 min, after which no additional adsorption takes place owing to the maximal occupancy of adsorption centers. Comparing the two adsorbents, S1@chitosan consistently shows a higher separation efficiency of Cd(II) ions than S1 across all time points. The

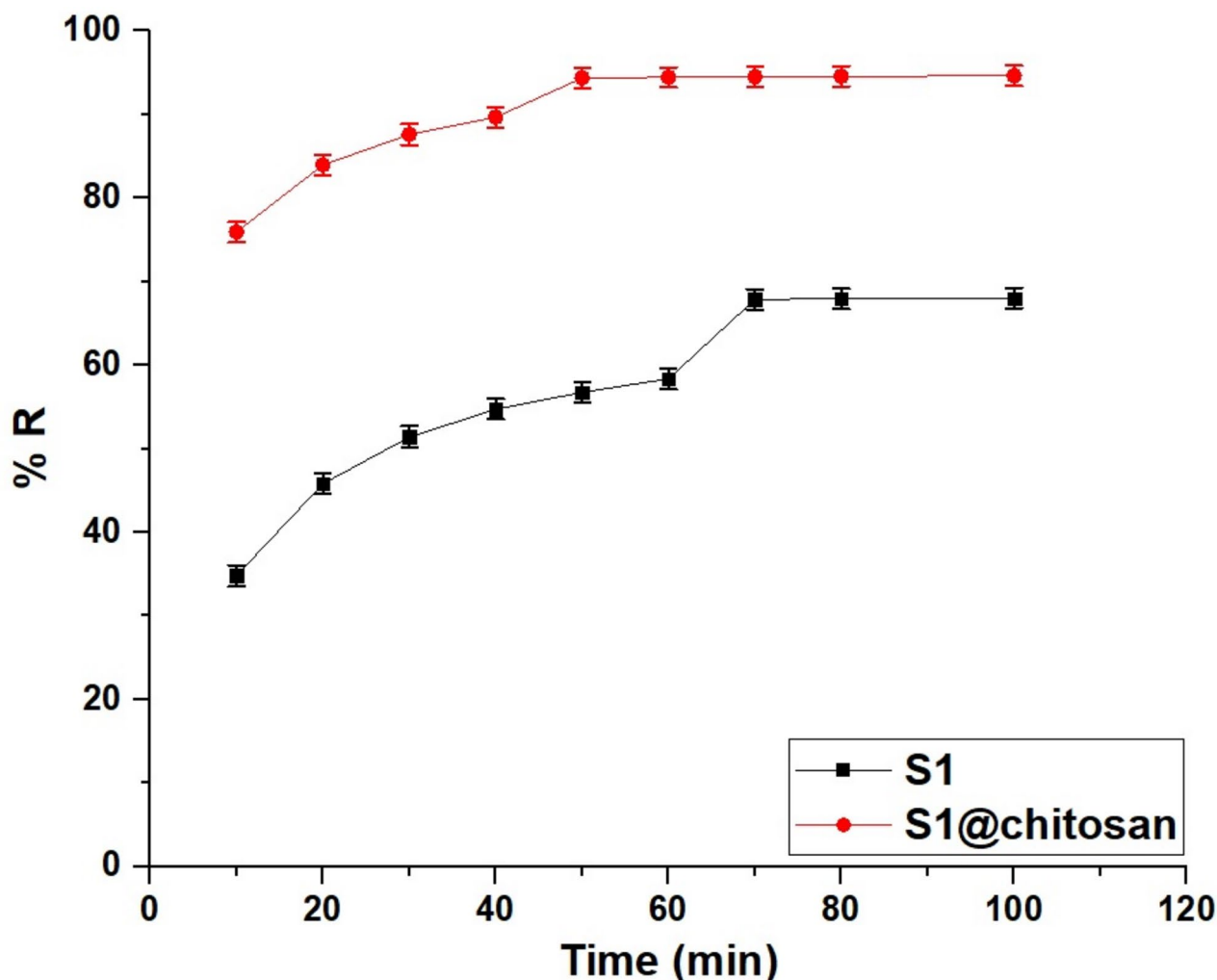


Fig. 8. Effect of time on the separation efficiency of Cd(II) ions utilizing S1 and S1@chitosan samples.

faster equilibrium time for S1@chitosan (50 min) compared to S1 (70 min) highlights the enhanced adsorption capacity and efficiency of S1@chitosan due to the combined mechanisms of ion exchange and complexation via the NH_2 and OH groups of chitosan. The results demonstrate that S1@chitosan not only reaches a higher separation efficiency but also does so in a significantly shorter time, making it a more effective adsorbent for Cd(II) ions.

The data were studied using the pseudo-1st -order as well as pseudo-2nd -order kinetic models as illustrated in Fig. 9A,B, respectively. The pseudo-1st -order model is represented by Eq. (7)^{35,36}.

$$\log(Q_e - Q_t) = \log Q_e - \frac{Z_1}{2.303}t \quad (7)$$

where, Q_e is the amount of adsorbate adsorbed at equilibrium, Q_t is the amount of adsorbate adsorbed at time t , and Z_1 is the rate constant of the pseudo-1st -order adsorption model.

Also, the pseudo-2nd -order model is represented by Eq. (8)^{35,37}.

$$\frac{t}{Q_t} = \frac{1}{Z_2 Q_e^2} + \frac{1}{Q_e}t \quad (8)$$

where, Z_2 is the rate constant of the pseudo-2nd -order adsorption model.

The constants Z_1 , Z_2 , and Q_e were established for each model and are presented in Table 4. The adsorption process aligns with the pseudo-2nd -order model, as indicated by the Q_{Exp} and R^2 values in Table 4. The experimental Q_{Exp} values for both S1 and S1@chitosan closely match the calculated Q_e sorption values, and the higher R^2 values in the pseudo-2nd -order model confirm a more accurate description of the separation mechanism.

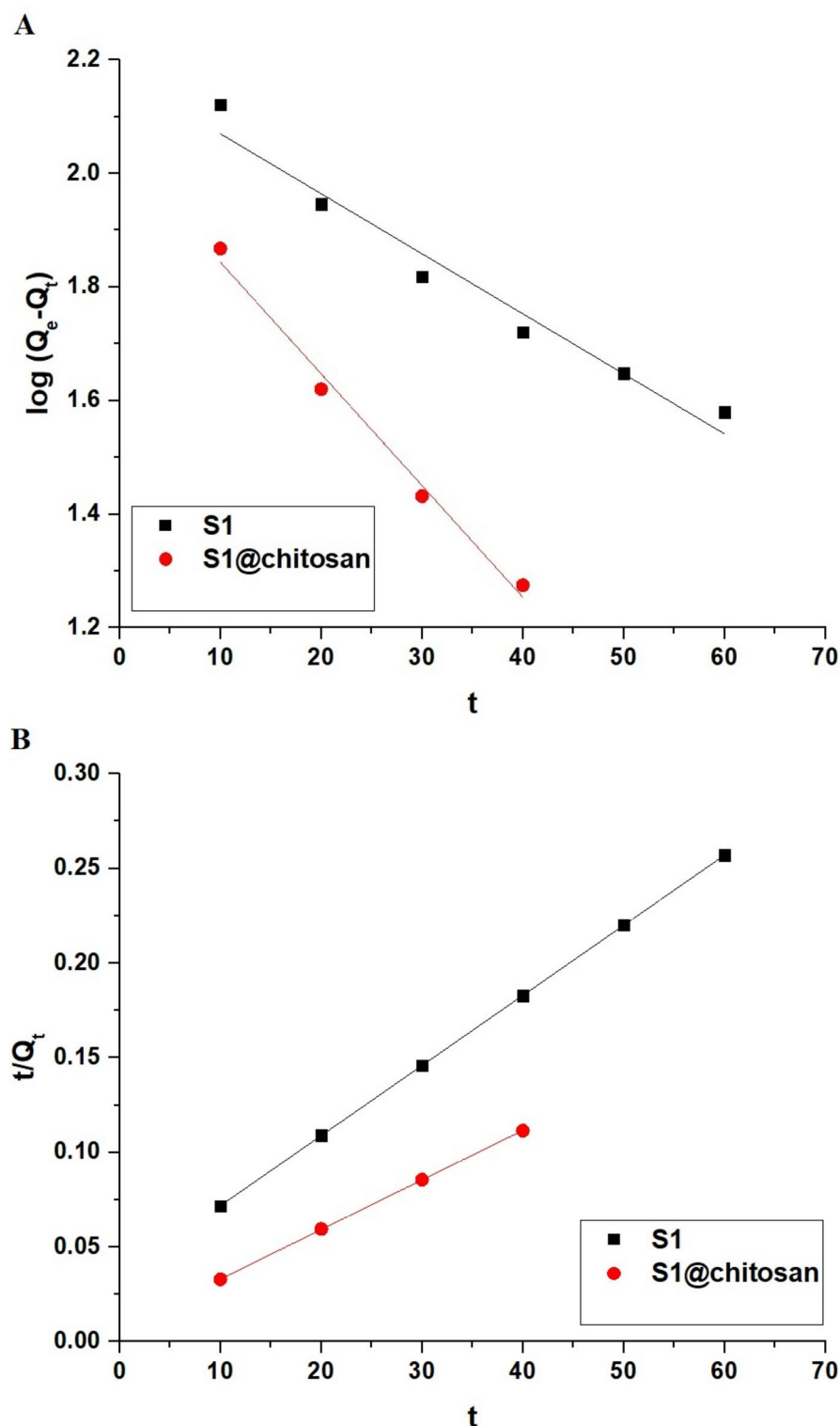


Fig. 9. (A) Pseudo-1st -order and (B) pseudo-2nd -order kinetic models for the adsorption of Cd(II) ions onto S1 and S1@chitosan adsorbents.

Effect of temperature

As depicted in Fig. 10, the results imply that the separation efficiency of Cd(II) ions by both S1 and S1@chitosan adsorbents decreases in response to temperature elevation, suggesting that the separation process is exothermic. At lower temperatures, the adsorbents have a higher affinity for Cd(II) ions, leading to greater separation efficiency, while at higher temperatures, the separation efficiency diminishes, likely due to the increased kinetic energy of the Cd(II) ions, which reduces their interaction with the adsorbent surfaces. At 298 K, as shown

Adsorbent	Q_{Exp} (mg/g)	Pseudo-1st-order			Pseudo-2nd-order		
		Z_1 (1/min)	Q_e (mg/g)	R^2	Z_2 (g/mg min)	Q_e (mg/g)	R^2
S1	271.50	0.02434	149.78	0.9562	0.0003928	270.27	0.9999
S1@chitosan	377.50	0.04528	109.71	0.9838	0.0009891	381.68	0.9999

Table 4. Kinetic parameters for the adsorption of Cd(II) ions onto S1 and S1@chitosan adsorbents according to the pseudo-1st -order as well as pseudo-2nd -order models.

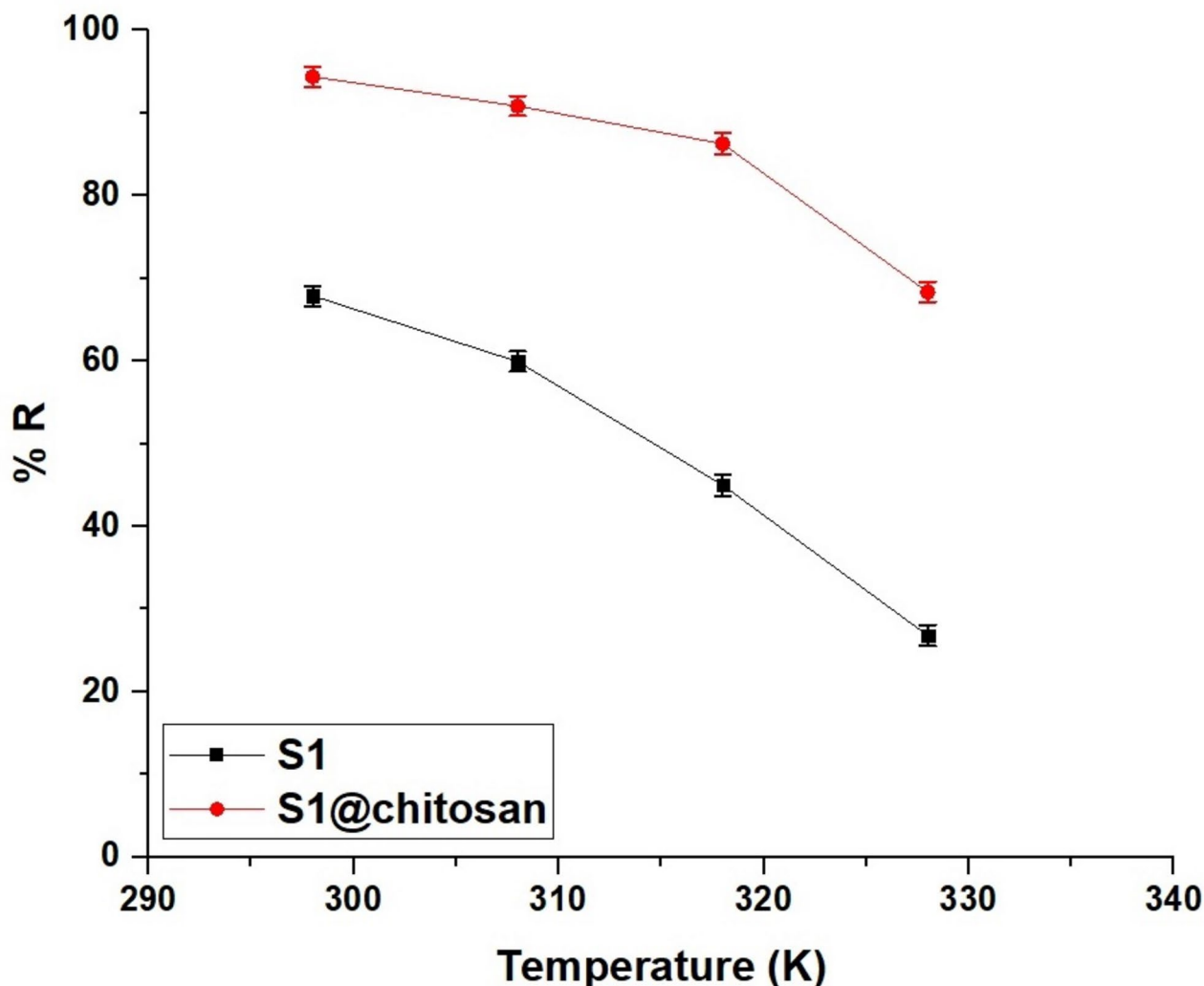


Fig. 10. Effect of temperature on the separation efficiency of Cd(II) ions utilizing S1 and S1@chitosan samples.

in Fig. 10, the separation efficiency is relatively high for both adsorbents, with S1 achieving 67.88% and S1@chitosan reaching 94.38%. This difference indicates that S1@chitosan, due to its enhanced functional groups, such as NH_2 and OH groups from chitosan, provides a greater number of active sites for adsorption, resulting in significantly higher efficiency compared to S1. At this temperature, the adsorption process is most favorable, and the higher efficiency of S1@chitosan underscores its superior performance in capturing Cd(II) ions. At 328 K, as depicted in Fig. 10, the separation efficiencies for both adsorbents decrease markedly, with S1 showing a separation efficiency of 26.81% and S1@chitosan achieving 68.33%. The significant reduction at this elevated temperature suggests that the thermal energy disrupts the adsorption interactions, such as ion exchange and complexation, between the Cd(II) ions and the adsorbent surfaces.

Figure 11 and Table 5 provide insights into the thermodynamic behavior of Cd(II) ion adsorption onto S1 and S1@chitosan adsorbents. The thermodynamic parameters were calculated using Eqs. (9–11). Equation (9) allows for the determination of the adsorption distribution constant (Z_d)³⁵.

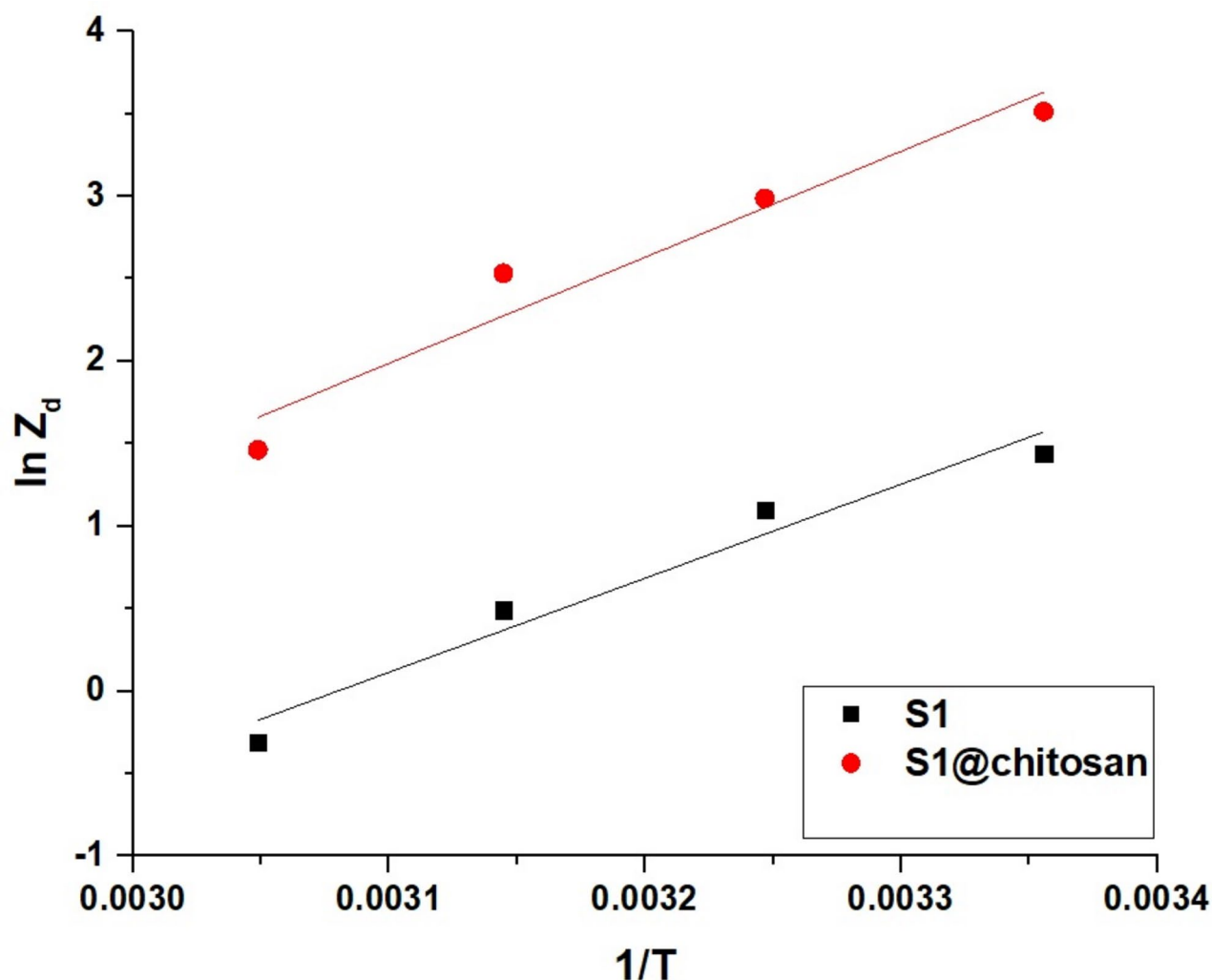


Fig. 11. Plot of $\ln Z_d$ versus $1/T$.

Adsorbent	ΔS° (KJ/molK)	ΔH° (KJ/mol)	ΔG° (KJ/mol)			
			298	308	318	328
S1	0.1467	- 47.63	- 91.34	- 92.81	- 94.27	- 95.74
S1@chitosan	0.1498	- 53.69	- 98.33	- 99.83	- 101.33	- 102.82

Table 5. Thermodynamic parameters (ΔS° , ΔH° , and ΔG°) for the adsorption of Cd(II) ions onto S1 and S1@chitosan adsorbents.

$$Z_d = \frac{Q_e}{C_e} \quad (9)$$

Equation (10) allows for the determination of ΔH° (enthalpy change) and ΔS° (entropy change) by constructing a linear plot of $\ln Z_d$ against $1/T$. From this plot, the slope corresponds to $\Delta H^\circ/R$ whereas the intercept represents $\Delta S^\circ/R$. R is the gas constant³⁸.

$$\ln Z_d = \frac{\Delta S^\circ}{R} - \frac{\Delta H^\circ}{RT} \quad (10)$$

Equation (11) determines ΔG° (Gibbs free energy change) as the difference between the enthalpy change (ΔH°) and the product of temperature (T) and entropy change (ΔS°)³⁸.

$$\Delta G^{\circ} = \Delta H^{\circ} - T\Delta S^{\circ} \quad (11)$$

The Van't Hoff plot in Fig. 11 shows the linear relationship between $\ln Z_d$ and $1/T$ for both adsorbents, reinforcing the exothermic nature of the adsorption process. The results in Table 5 indicate that the adsorption process for both S1 and S1@chitosan is chemical in nature, as indicated by the values of ΔH° being greater than 40 kJ/mol. The process is exothermic, as reflected by the negative ΔH° values of -47.63 kJ/mol for S1 and -53.69 kJ/mol for S1@chitosan, and spontaneous, as shown by the negative ΔG° values at all temperatures studied. The entropy changes (ΔS°) are positive for both adsorbents, with values of 0.1467 kJ/molK for S1 and 0.1498 kJ/molK for S1@chitosan, indicating that the adsorption is feasible.

Effect of concentration

Figure 12 show the effect of varying concentrations of Cd(II) ions on the separation efficiency using S1 and S1@chitosan adsorbents. As the concentration of Cd(II) ions increases from 50 to 300 mg/L, the separation efficiency decreases for both adsorbents. At a lower concentration of 50 mg/L, S1 achieves a separation efficiency of 93.00%, while S1@chitosan shows a slightly higher efficiency of 97.90%, indicating that both adsorbents are highly effective at lower concentrations. As the concentration increases to 300 mg/L, the separation efficiencies decline to 46.01% for S1 and 63.42% for S1@chitosan, reflecting a major reduction in performance. The data show that S1@chitosan consistently exhibits a higher separation efficiency than S1 across all concentrations, indicating that the presence of chitosan enhances the adsorption capacity and effectiveness of the adsorbent. The overall trend suggests that while both adsorbents are effective at lower concentrations of Cd(II) ions, their efficiency decreases with increasing concentration, likely due to the saturation of available adsorption sites on the surface of the adsorbents.

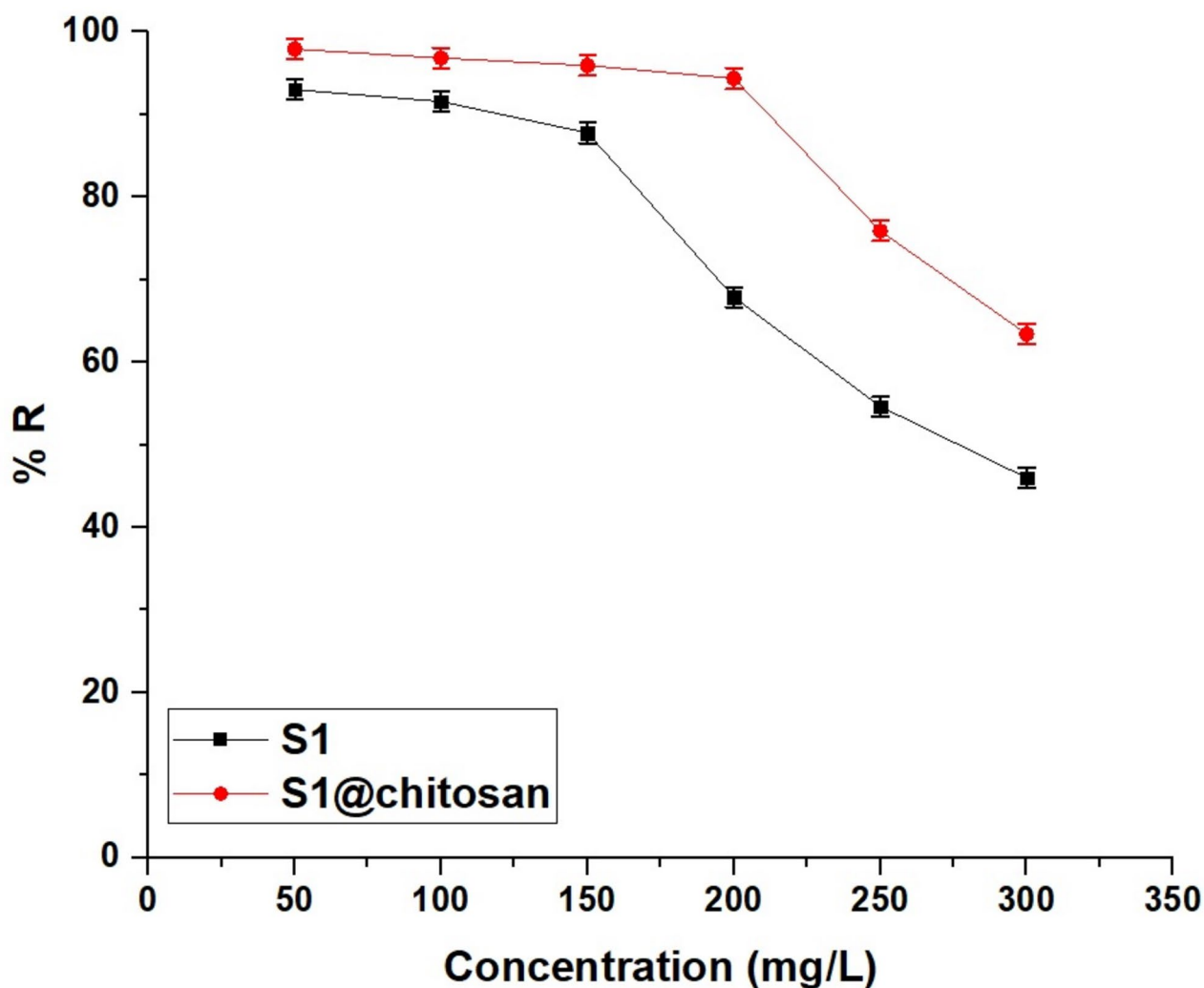


Fig. 12. Effect of preliminary concentration on the separation efficiency of Cd(II) ions utilizing S1 and S1@chitosan samples.

The data were studied using the Langmuir and Freundlich isotherm models to describe the adsorption behavior of Cd(II) ions onto S1 and S1@chitosan adsorbents, as illustrated in Fig. 13A,B, respectively. Also, the Langmuir isotherm is represented by Eq. (12)^{35,39}.

$$\frac{C_e}{Q_e} = \frac{1}{Z_3 Q_{max}} + \frac{C_e}{Q_{max}} \quad (12)$$

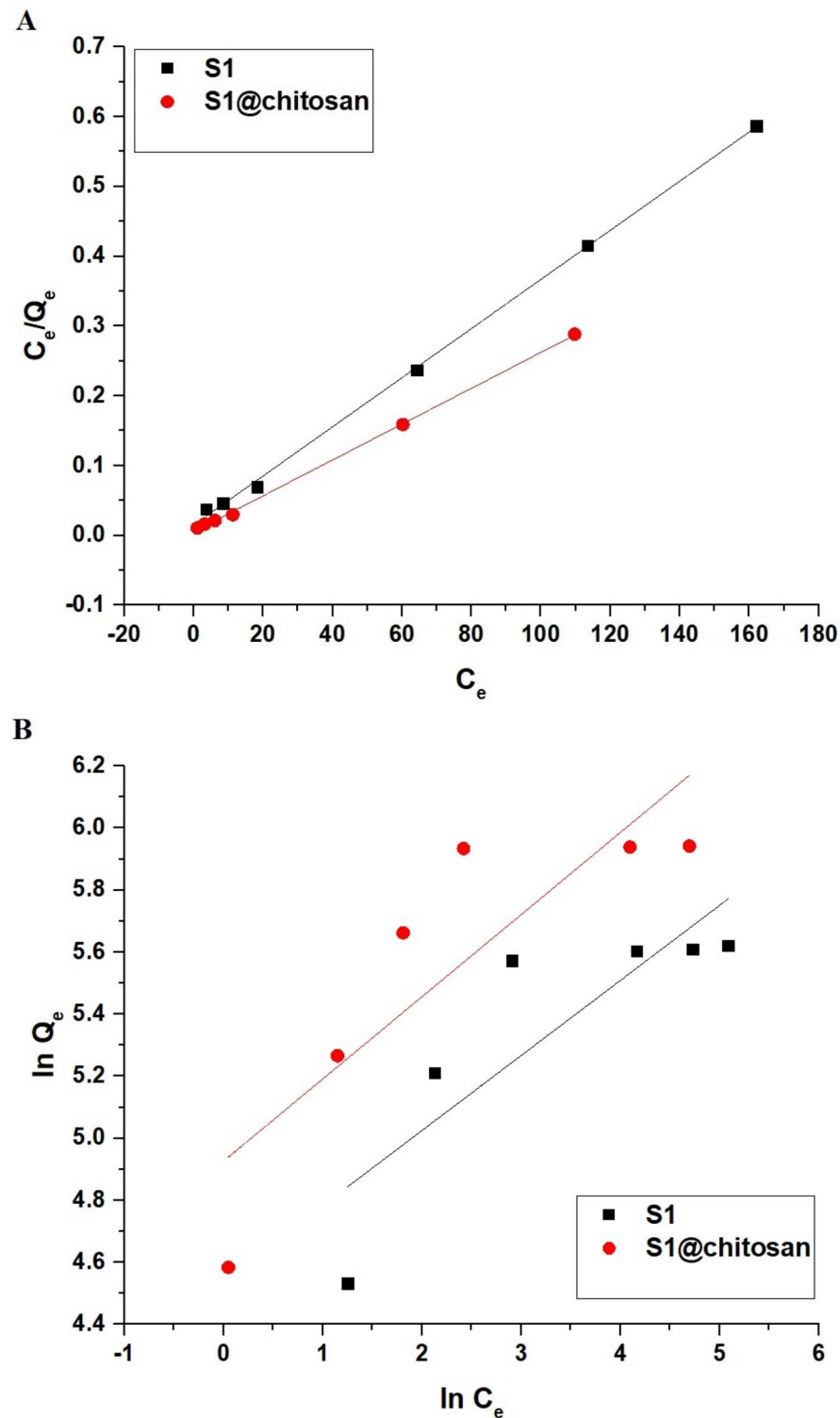


Fig. 13. (A) Langmuir and (B) Freundlich isotherms for the separation of Cd(II) ions utilizing S1 and S1@chitosan adsorbents.

Adsorbent	Langmuir			Freundlich			
	Q_{\max} (mg/g)	R^2	Z_3 (L/mg)	Z_4 (mg/g)(L/mg) ^{1/n}	Q_{\max} (mg/g)	1/n	R^2
S1	284.09	0.9989	0.2333	93.81	337.87	0.2418	0.6547
S1@chitosan	389.11	0.9993	0.4573	137.92	560.72	0.2647	0.6744

Table 6. Equilibrium parameters for the separation of Cd(II) ions utilizing S1 and S1@chitosan adsorbents according to the Langmuir as well as Freundlich isotherms.

Adsorbent	Q_{\max} (mg/g)	Refs.
Chitosan/alginate beads	207.00	41
MnFe ₂ O ₄ @SBA-15-(CH ₂) ₃ -adenine	29.62	42
Phosphorylated chitosan/CoFe ₂ O ₄ composite	71.53	43
Polyaniline-grafted-chitosan	12.87	44
Chitosan/perlite beads	178.6	45
Chitosan/polyvinyl alcohol blend beads	142.90	46
Faujasite zeolite	74.074	47
Iron oxide/activated carbon composite	18.59	48
Zero-valent iron nanoparticles	102.00	49
Chitosan/silica composite	11.54	50
Graphene oxide-silica-chitosan composite	126.58	51
S1	284.09	This study
S1@chitosan	389.11	This study

Table 7. Maximum separation capacities (Q_{\max}) of several adsorbents utilized to remove Cd(II) ions.

where, Q_{\max} is the maximum adsorption capacity and Z_3 is the Langmuir constant.
The Freundlich isotherm is represented by Eq. (13)^{12,35}.

$$\ln Q_e = \ln Z_4 + \frac{1}{n} \ln C_e \tag{13}$$

where, Z_4 and 1/n are the Freundlich constants indicating adsorption capacity and intensity, respectively. Additionally, the maximum adsorption capacity (Q_{\max}) can be calculated using Eq. (14)⁴⁰.

$$Q_{\max} = Z_4 \left(C_o^{\frac{1}{n}} \right) \tag{14}$$

The separation process follows the Langmuir isotherm model based on the higher R^2 values observed in Table 6. For S1, the Langmuir model shows an R^2 value of 0.9989, while the Freundlich model has a lower R^2 value of 0.6547. Similarly, for S1@chitosan, the R^2 value is 0.9993 for the Langmuir equilibrium model, in comparison with 0.6744 for the Freundlich equilibrium model, indicating a better fit with the Langmuir isotherm. These results suggest that the adsorption of Cd(II) ions onto both S1 and S1@chitosan is more accurately described by the Langmuir equilibrium isotherm, which proposes a single-layer adsorption on a uniform surface.

Table 7 shows that the S1@chitosan composite from this study has the highest maximum separation capacity for Cd(II) ions (389.11 mg/g), surpassing all other listed adsorbents^{41–49}. The S1 adsorbent also demonstrates a strong performance with a capacity of 284.09 mg/g, which is higher than many conventional and advanced materials, such as chitosan/alginate beads and chitosan/polyvinyl alcohol blend beads. These results highlight the superior adsorption efficiency of S1 and S1@chitosan compared to other reported materials. Several studies have explored silica–chitosan composites for Cd(II) removal. For example, Lachhimpui et al. synthesized a mesoporous silica–chitosan composite, achieving an adsorption capacity of 11.54 mg/g for Cd(II) ions⁵⁰. Similarly, Azizkhani et al. developed a graphene oxide-silica-chitosan composite, reporting a Cd(II) adsorption capacity of 126.58 mg/g⁵¹. While these materials demonstrated effective Cd(II) removal, their adsorption capacities remain significantly lower than that of S1@chitosan (389.11 mg/g). The superior performance of S1@chitosan can be attributed to the unique combination of sodium iron oxide silicate and chitosan, which enhances ion-exchange properties and provides additional active sites for adsorption. Additionally, previous studies primarily focused on adsorption through surface complexation, whereas S1@chitosan utilizes both ion exchange and complexation mechanisms, leading to enhanced Cd(II) removal efficiency. Furthermore, S1@chitosan exhibits excellent reusability, maintaining high adsorption efficiency over multiple cycles, whereas previous silica-based composites showed a decline in performance after repeated use.

Contrary to common assumptions, both chitosan and sodium metasilicate are affordable and widely available materials, making the synthesis of the S1@chitosan composite economically feasible. Furthermore, the prepared

adsorbents exhibit significantly higher adsorption capacities than conventional materials such as clay and biochar, making them more efficient for Cd(II) removal. This high efficiency justifies their use despite potential concerns about material costs. Additionally, the synthesis process is straightforward and does not require high-energy consumption or expensive reagents, which enhances the scalability of this approach. Future research could focus on optimizing synthesis conditions to further reduce costs, exploring industrial-scale applications, and conducting a detailed cost-benefit analysis to confirm the long-term viability of S1@chitosan as a sustainable and efficient adsorbent.

Effect of interference

A binary adsorption study was conducted to evaluate the impact of interfering ions on Cd(II) adsorption using S1 and S1@chitosan. The experiments were performed at pH 7.5 and 298 K with an initial Cd(II) concentration of 200 mg/L maintaining a 1:1 molar ratio of Cd(II) to each competing ion. The interfering ions included Na⁺, K⁺, Mg²⁺, Ca²⁺, Cl⁻, NO₃⁻, and SO₄²⁻ representing common cations and anions found in aqueous environments. Batch adsorption experiments were conducted by adding 0.05 g of each adsorbent to 100 mL of Cd(II) solution containing the competing ion. The mixtures were stirred for 50 min for S1@chitosan and 70 min for S1 until equilibrium was achieved. The final Cd(II) concentration was measured using atomic absorption spectrophotometry and adsorption capacities were determined based on mass balance calculations. The results are summarized in Table 8. The results indicate that monovalent cations such as Na⁺ and K⁺ had minimal effects on Cd(II) adsorption, causing slight reductions in adsorption capacities for both S1 and S1@chitosan. Similarly, the presence of Cl⁻ and NO₃⁻ exhibited negligible interference. In contrast, divalent cations, particularly Mg²⁺ and Ca²⁺, significantly reduced the adsorption capacity of both materials. The highest reduction was observed in the presence of Ca²⁺, which led to a decrease of 26.6 mg/g for S1 and 28.72 mg/g for S1@chitosan. The pronounced inhibitory effect of divalent cations can be attributed to competitive adsorption, where Mg²⁺ and Ca²⁺ occupy active adsorption sites, limiting Cd(II) binding. Additionally, the stronger electrostatic interactions of these cations with negatively charged functional groups on the adsorbent surface further hinder Cd(II) adsorption. These findings suggest that S1 and S1@chitosan exhibit high selectivity toward Cd(II) in the presence of monovalent ions, while divalent cations, particularly Ca²⁺, significantly interfere with the adsorption process of Cd(II) ions.

Evaluation of regeneration and reusability

Figure 14 show the desorption efficiency (% D) of Cd(II) ions from S1 and S1@chitosan adsorbents at different concentrations of HCl. At a lower HCl concentration of 0.50 M, S1 achieves a desorption efficiency of 88.44%, while S1@chitosan shows a lower efficiency of 74.79%, indicating that S1 is more effective at desorbing Cd(II) ions under milder acidic conditions. If the HCl concentration is increased to 1.0 M, the desorption efficiencies for both adsorbents are nearly identical, with S1 reaching 92.28% and S1@chitosan achieving 92.95%, suggesting that the desorption capability of S1@chitosan improves significantly at this concentration. At the highest tested concentration of 1.50 M HCl, both S1 and S1@chitosan exhibit excellent desorption efficiencies, with S1 reaching 99.61% and S1@chitosan achieving 99.71%. This indicates that at higher acid concentrations, both adsorbents are equally effective in desorbing Cd(II) ions, with only a slight difference between them. Overall, the desorption efficiency increases with the concentration of HCl, and both adsorbents perform optimally at 1.50 M, although S1@chitosan demonstrates a slightly higher desorption efficiency at this concentration. HCl was specifically chosen due to its strong acid dissociation, ensuring complete protonation of functional groups on the adsorbent surface, which facilitates the release of Cd(II) ions. Additionally, HCl provides a high ionic strength, effectively breaking interactions between the adsorbed Cd(II) ions and the functional sites. In comparison, HNO₃ and H₂SO₄ were tested but resulted in significantly lower desorption efficiencies. The desorption efficiency of Cd(II) ions using HNO₃ and H₂SO₄ was found to be much lower than that achieved with HCl. This is likely due to the weaker ability of these acids to disrupt the bonds between Cd(II) and the adsorbent, as well as possible secondary interactions that may hinder the complete release of Cd(II). Given these findings, HCl was determined to be the most effective eluent for the desorption process.

Figure 15 shows the reusability performance of S1 and S1@chitosan adsorbents for removing Cd(II) ions over five consecutive adsorption-desorption cycles. In the initial cycle (cycle 0), S1 achieves a removal efficiency of 67.88%, while S1@chitosan demonstrates a significantly higher removal efficiency of 94.38%, indicating the superior initial adsorption capacity of S1@chitosan. After the first cycle, the removal efficiency of both adsorbents slightly decreases, with S1 maintaining a removal efficiency of 67.09% and S1@chitosan achieving 93.73%. As

Interfering ions	Q of S1 (mg/g)	Q of S1@chitosan (mg/g)	Reduction in Q of S1 (mg/g)	Reduction in Q of S2 (mg/g)
None (control)	271.5	377.5	–	–
Na ⁺	268.21	373.85	3.29	3.65
K ⁺	267.98	373.42	3.52	4.08
Mg ²⁺	250.43	356.2	21.07	21.3
Ca ²⁺	244.9	348.78	26.6	28.72
Cl ⁻	269.87	375.99	1.63	1.51
NO ₃ ⁻	266.75	372.5	4.75	5.0

Table 8. Effect of interfering ions on adsorption of Cd(II) ions using S1 and S1@chitosan composite.

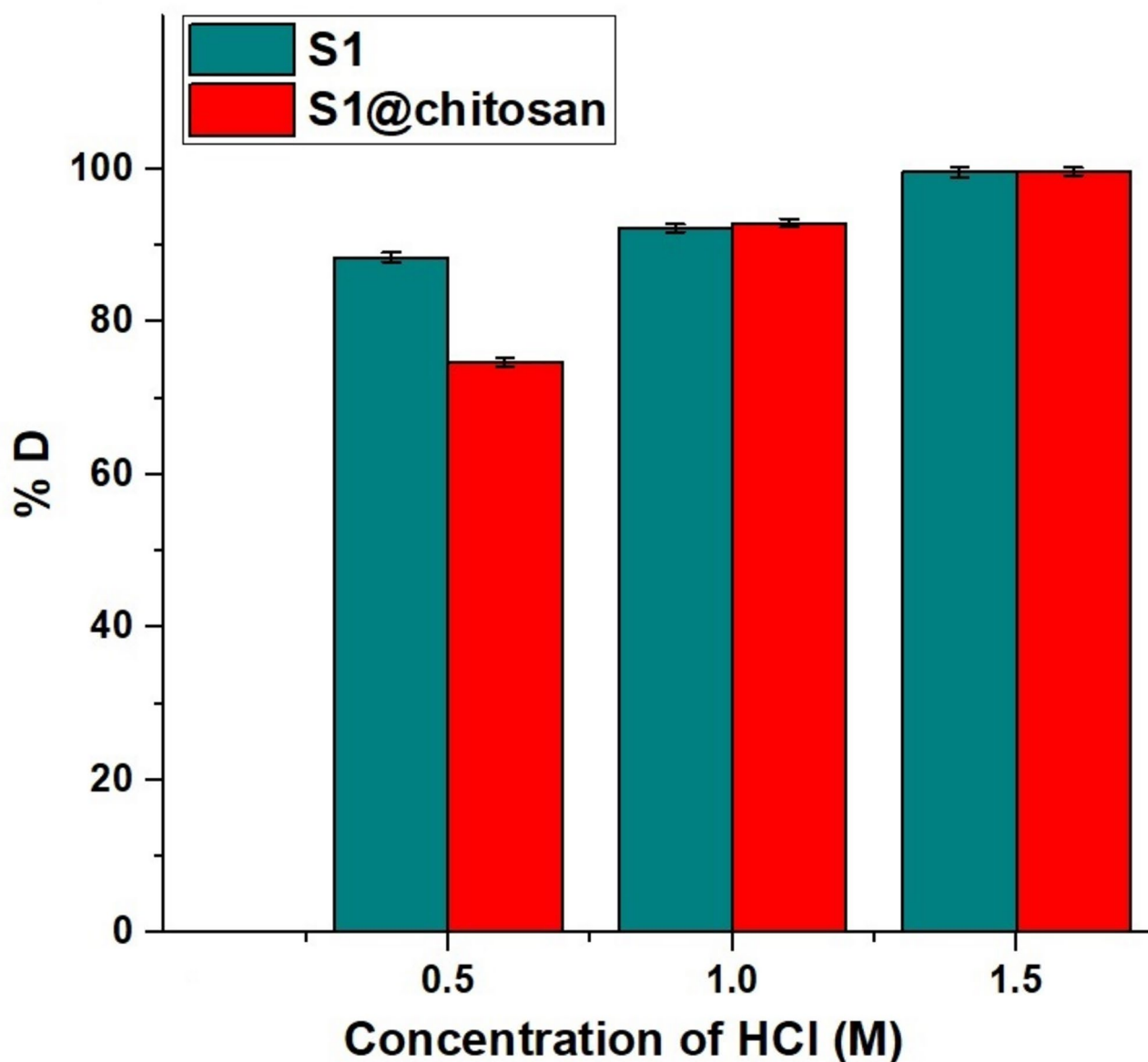


Fig. 14. Desorption efficiency (% D) of Cd(II) ions from S1 and S1@chitosan adsorbents at varying concentrations of HCl.

the cycles progress, the removal efficiencies for both adsorbents gradually decline. By the second cycle, S1 has a removal efficiency of 66.23%, while S1@chitosan still retains a high efficiency of 91.64%. By the third cycle, S1 shows a further reduction to 64.66%, whereas S1@chitosan maintains a relatively high efficiency of 90.67%. This trend continues through the fourth and fifth cycles, with S1 decreasing to 63.05% and 61.58%, respectively, and S1@chitosan decreasing to 89.89% and 88.10%. Throughout all five cycles, S1@chitosan consistently exhibits a higher removal efficiency compared to S1, demonstrating its greater stability and effectiveness in the repeated adsorption-desorption process. This suggests that S1@chitosan is a more durable and efficient adsorbent for separation of Cd(II) ions in multiple reuse cycles.

Conclusions

This study successfully synthesized and evaluated a sodium iron oxide silicate@amorphous sodium iron silicate product (S1) and its chitosan composite (S1@chitosan) for the effective removal of Cd(II) ions from aqueous media. The optimized adsorption conditions were determined to be pH 7.50, a contact time of 50 min for S1@chitosan (70 min for S1), and a temperature of 298 K. The S1@chitosan composite demonstrated a significantly higher adsorption capacity (389.11 mg/g) than S1 (284.09 mg/g), highlighting the synergistic effect of chitosan functionalization. Adsorption followed the pseudo-second-order kinetic model, confirming a chemisorption mechanism, and was best described by the Langmuir isotherm, indicating monolayer adsorption. Thermodynamic analysis confirmed that the process is spontaneous and exothermic, suggesting strong

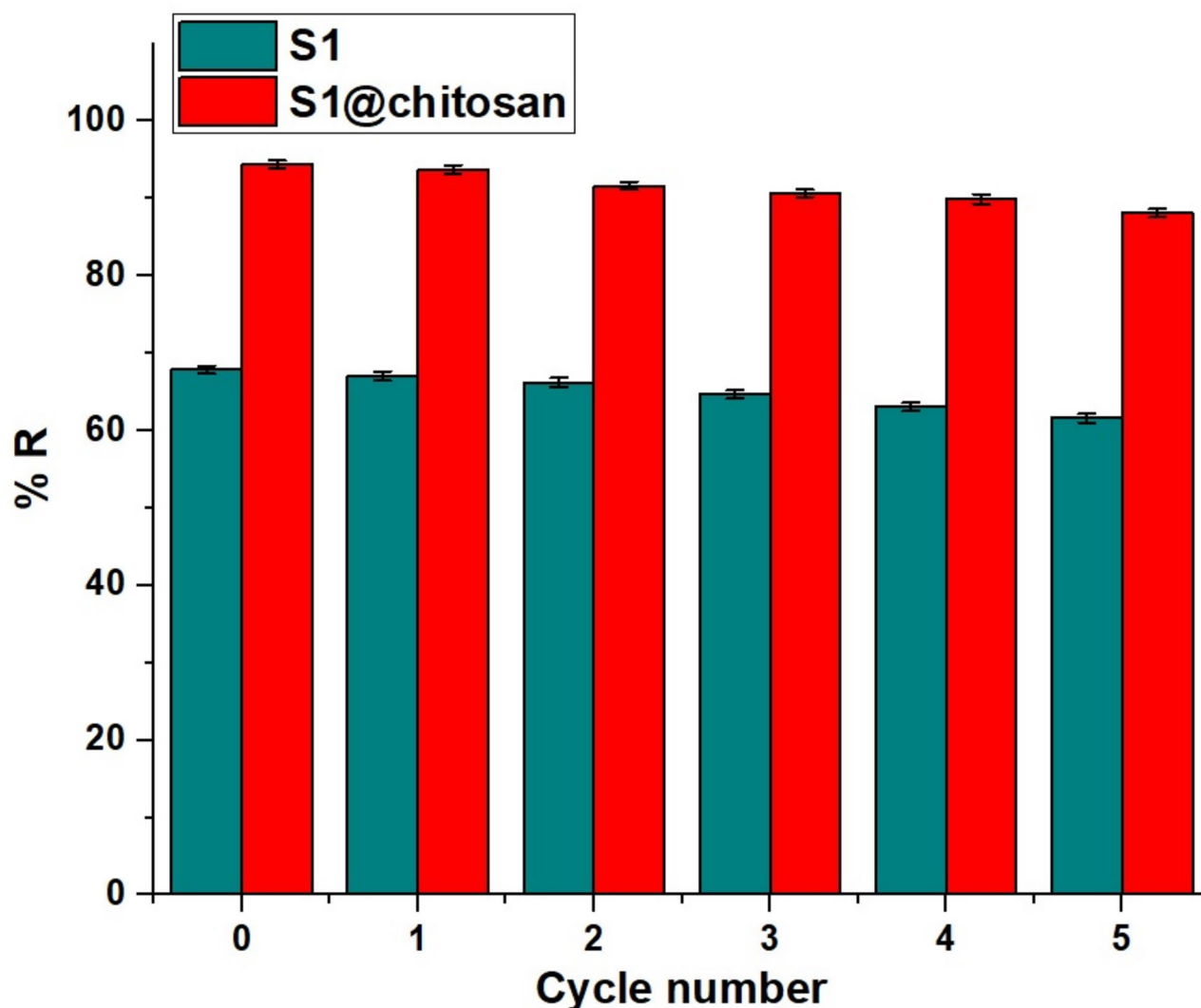


Fig. 15. Reusability of S1 and S1@chitosan adsorbents for the separation of Cd(II) ions over multiple adsorption-desorption cycles.

interactions between Cd(II) ions and the composite material. Furthermore, the reusability tests demonstrated that S1@chitosan retained its high adsorption efficiency over multiple cycles, emphasizing its potential as a cost-effective and sustainable adsorbent for heavy metal remediation. These findings underscore the promising application of S1@chitosan for water purification, offering an efficient, reusable, and environmentally friendly solution for Cd(II) removal from contaminated water sources.

Data availability

All data produced or examined in this study are fully presented within this published article.

Received: 9 January 2025; Accepted: 17 April 2025

Published online: 12 May 2025

References

1. Hazirah, F., Hafiz, M., Othman, D. & Jannah, N. Journal of the Taiwan Institute of chemical engineers Hydroxyapatite-based materials for adsorption, and adsorptive membrane process for heavy metal removal from wastewater: Recent progress, bottleneck and opportunities. *J. Taiwan. Inst. Chem. Eng.* **164**, 105668 (2024).
2. Joshi, N. C. et al. Removal of heavy metals using cellulose-based materials: A mini-review. *Environ. Nanotechnol. Monit. Manag.* **21**, 100942 (2024).
3. Feisal, N. A. S., Kamaludin, N. H. & Ahmad, M. A. Tengku Ibrahim, T. N. B. A comprehensive review of nanomaterials for efficient heavy metal ions removal in water treatment. *J. Water Process. Eng.* **64**, 105566 (2024).
4. Senthil Rathi, B. et al. Recent research progress on the removal of heavy metals from wastewater using modified zeolites: A critical review. *Desalin. Water Treat.* **319**, 100573 (2024).
5. Ismail, U. M., Vohra, M. S. & Onaizi, S. A. Adsorptive removal of heavy metals from aqueous solutions: Progress of adsorbents development and their effectiveness. *Environ. Res.* **251**, 118562 (2024).

6. Yu, T. et al. Journal of industrial and engineering chemistry tourmaline for heavy metals removal in wastewater treatment: A review. *J. Ind. Eng. Chem.* **131**, 44–53 (2024).
7. Chen, Y. et al. Porous sodium alginate/cellulose nanofiber composite hydrogel microspheres for heavy metal removal in wastewater. *Int. J. Biol. Macromol.* **278**, 135000 (2024).
8. Li, S. et al. Nanoconfined polyethyleneimine in mesoporous MCM-41 silica for heavy metal ions removal. *Sep. Purif. Technol.* **353**, 128421 (2025).
9. Gozali Balkanloo, P., Poursattar Marjani, A. & Mahmoudian, M. Fabrication, characterization, and performance evaluation of polysulfone nanocomposite membranes containing different sizes of ZIF-8 to desalination and heavy metals removal from wastewater. *Chem. Eng. J.* **496**, 153835 (2024).
10. Phouthavong, V. et al. Removal of heavy metals by BEA zeolite/Fe₃O₄ composite prepared via dry-gel conversion method using agrowaste-derived Raw material. *Solid State Sci.* **149**, 107473 (2024).
11. Singh, D. et al. Citric acid coated magnetic nanoparticles: Synthesis, characterization and application in removal of Cd(II) ions from aqueous solution. *J. Water Process. Eng.* **4**, 233–241 (2014).
12. Hu, L. et al. Synthesis of ZIF-8 in high yield and simultaneous removal of Mn(II), Cu(II), and Cd(II): Performance and mechanism. *Chem. Eng. Res. Des.* **208**, 217–226 (2024).
13. Nabipour, H., Rohani, S., Batool, S. & Yusuff, A. S. An overview of the use of water-stable metal-organic frameworks in the removal of cadmium ion. *J. Environ. Chem. Eng.* **11**, 109131 (2023).
14. Ma, J., Li, Q., Zhang, X. & Yu, F. Recent advances and future challenges in selective removal of calcium and magnesium ions with capacitive deionization. *Coord. Chem. Rev.* **517**, 216001 (2024).
15. Chen, Q. et al. Comparison of heavy metal removals from aqueous solutions by chemical precipitation and characteristics of precipitates. *J. Water Process. Eng.* **26**, 289–300 (2018).
16. Xiang, H., Min, X., Tang, C. J., Sillanpää, M. & Zhao, F. Recent advances in membrane filtration for heavy metal removal from wastewater: A mini review. *J. Water Process. Eng.* **49**, 103023 (2022).
17. Ghamari, F., Negar, Z. A., Arjomandi, J. & Shi, H. Novel polyaniline/8-hydroxyquinoline composite electrode materials for simultaneous electrochemical removal of heavy metal ions from water resources. *J. Environ. Chem. Eng.* **10**, 108830 (2022).
18. Nizam, T., Krishnan, K. A., Joseph, A. & Krishnan, R. R. Isotherm, kinetic and thermodynamic modelling of liquid phase adsorption of the heavy metal ions Zn(II), Pb(II) and Cr(VI) onto MgFe₂O₄ nanoparticles. *Groundw. Sustain. Dev.* **25**, 101120 (2024).
19. Drużyński, S., Mazurek, K., Kielkowska, U., Ciesielczyk, F. & Jesionowski, T. Adsorption of Cu(II) and Zn(II) onto ZrO₂-SiO₂ composite: Characteristics, mechanism and application in wastewater treatment. *Desalin. Water Treat.* **320**, 100657 (2024).
20. Archana, Yadav, N., Thakur, A., Singh, S. & Srivastava, S. A comparative study of calcium oxide nanoparticle and its ferrite (CaO/Fe₂O₃) nanocomposite for removal of zinc and nickel from electroplating effluent. *Inorg. Chem. Commun.* **167**, 112746 (2024).
21. Gupta, K., Joshi, P., Gusain, R. & Khatri, O. P. Recent advances in adsorptive removal of heavy metal and metalloid ions by metal oxide-based nanomaterials. *Coord. Chem. Rev.* **445**, 214100 (2021).
22. Li, M. et al. Recent advances in application of iron-manganese oxide nanomaterials for removal of heavy metals in the aquatic environment. *Sci. Total Environ.* **819**, 153157 (2022).
23. Jayalakshmi, R., Jeyanthi, J. & Aswin Sidhaarth, K. R. Versatile application of Cobalt ferrite nanoparticles for the removal of heavy metals and dyes from aqueous solution. *Environ. Nanotechnol. Monit. Manag.* **17**, 100659 (2022).
24. Abdelrahman, E. A., El-Reash, A., Youssef, Y. G., Kotp, H. M., Hegazey, R. M. & Y. H. & Utilization of rice husk and waste aluminum cans for the synthesis of some nanosized zeolite, zeolite/zeolite, and geopolymer/zeolite products for the efficient removal of Co(II), Cu(II), and Zn(II) ions from aqueous media. *J. Hazard. Mater.* **401**, 123813 (2021).
25. Abdelrahman, E. A. & Subaihi, A. Application of geopolymers modified with Chitosan as novel composites for efficient removal of Hg(II), Cd(II), and Pb(II) ions from aqueous media. *J. Inorg. Organomet. Polym. Mater.* **30**, 2440–2463 (2020).
26. Jin, J. et al. Magnetic-responsive CNT/chitosan composite as stabilizer and adsorbent for organic contaminants and heavy metal removal. *J. Mol. Liq.* **334**, 116087 (2021).
27. Rajamani, M. & Rajendrakumar, K. Chitosan-boehmite desiccant composite as a promising adsorbent towards heavy metal removal. *J. Environ. Manag.* **244**, 257–264 (2019).
28. Feng, G. et al. Magnetic natural composite Fe₃O₄-chitosan@bentonite for removal of heavy metals from acid mine drainage. *J. Colloid Interface Sci.* **538**, 132–141 (2019).
29. Bulin, C. Adsorption mechanism and removal efficiency of magnetic graphene oxide-chitosan hybrid on aqueous Zn(II). *Int. J. Biol. Macromol.* **241**, 124588 (2023).
30. Salih, S. S. et al. Chitosan-vermiculite composite adsorbent: Preparation, characterization, and competitive adsorption of Cu(II) and Cd(II) ions. *J. Water Process. Eng.* **59**, 105044 (2024).
31. Jawed, A., Sharad, A., Chutani, A., Pandey, L. M. & Mehak & Amine functionalized Fe(III)-doped-ZnO nanoparticles based alginate beads for the removal of Cu(II) from aqueous solution. *Nano-Struct. Nano-Objects.* **38**, 101199 (2024).
32. Sun, Y. P., Wang, G., Guo, Y. L. & Zhu, X. Y. An eco-friendly wheat straw adsorbent functionalized with mercaptopropionyl for the removal of Cu(II) from aqueous solution. *Chem. Eng. Sci.* **299**, 120454 (2024).
33. Al-wasidi, A. S., Katouah, H. A., Saad, F. A. & Abdelrahman, E. A. Functionalization of silica nanoparticles by 5-Chloro-8-quinolinol as a new nanocomposite for the efficient removal and preconcentration of Al³⁺ ions from water samples. *ACS Omega.* **8**, 15276–15287 (2023).
34. Al-Wasidi, A. S., Khairy, M., Abdulkhair, B. Y. & Abdelrahman, E. A. Efficient disposal of basic Fuchsin dye from aqueous media using ZrO₂/MgMn₂O₄/Mg(Mg_{0.333}Mn_{1.333})O₄ as a novel and facilely synthesized nanocomposite. *Inorganics* **11**, 363 (2023).
35. El, N., Abdalla, S., Ikhlās, M. K. & Ehab, A. M. Facile synthesis of sodium Iron silicate / sodium Iron oxide silicate nanostructures from canned beans and rice husk wastes for efficient removal of cd(II) ions from aqueous media. *Silicon* **16**, 2955–2970 (2024).
36. Qin, H. et al. Removal of Cu(II) by sodium hexametaphosphate and nano zero-valent iron modified calcium bentonite: Characteristic, adsorption performance and mechanism. *J. Environ. Manag.* **358**, 120866 (2024).
37. Jasem-Feisal, A., Amiripour, F. & Ghasemi, S. MOF-derived Co-Al layered double hydroxide modified rice husk Biochar nanohybrid for efficient removal of Cu(II) from wastewater. *J. Water Process. Eng.* **64**, 105612 (2024).
38. Al-Wasidi, A. S., Basha, M. T., Alghanmi, R. M., Al-Farraj, E. S. & Abdelrahman, E. A. Facile synthesis and characterization of sodium magnesium silicate hydrate/sodium magnesium silicate hydroxide as novel nanostructures for the efficient removal of methylene blue dye from aqueous media. *J. Inorg. Organomet. Polym. Mater.* **33**, 1005–1015 (2023).
39. Salem, M. A., Awad, M. K., Sleet, R. K. & El-Ghobashy, M. A. Adsorptive dye removal by Cu(II)-modified silica-alumina/polyaniline nanocomposite. *Mater. Chem. Phys.* **325**, 129795 (2024).
40. Al-wasidi, A. S. & Abdelrahman, E. A. Simple synthesis and characterization of Cobalt ferrite nanoparticles for the successful adsorption of Indigo Carmine dye from aqueous media. *Inorganics* **11**, 453 (2023).
41. Kuczajowska-Zadrozna, M., Filipkowska, U. & Jóźwiak, T. Adsorption of Cu(II) and Cd(II) from aqueous solutions by Chitosan immobilized in alginate beads. *J. Environ. Chem. Eng.* **8**, 103878 (2020).
42. Badvi Loulic, F., Shirazi, H. S. M., Miralinaghi, R., Ahmad Panahi, M., Moniri, E. & H. & Highly efficient removal of toxic As(V), Cd(II), and Pb(II) ions from water samples using MnFe₂O₄@SBA-15-(CH₂)₃-adenine as a recyclable bio-nano-adsorbent. *Microporous Mesoporous Mater.* **356**, 112567 (2023).
43. Wu, D. et al. Phosphorylated chitosan/CoFe₂O₄ composite for the efficient removal of Pb(II) and Cd(II) from aqueous solution: Adsorption performance and mechanism studies. *J. Mol. Liq.* **277**, 181–188 (2019).

44. Karthik, R. & Meenakshi, S. Removal of Pb(II) and Cd(II) ions from aqueous solution using polyaniline grafted Chitosan. *Chem. Eng. J.* **263**, 168–177 (2015).
45. Hasan, S. et al. Adsorption of divalent cadmium (Cd(II)) from aqueous solutions onto chitosan-coated perlite beads. *Ind. Eng. Chem. Res.* **45**, 5066–5077 (2006).
46. Kumar, M., Tripathi, B. P. & Shahi, V. K. Crosslinked Chitosan/polyvinyl alcohol blend beads for removal and recovery of Cd(II) from wastewater. *J. Hazard. Mater.* **172**, 1041–1048 (2009).
47. Joseph, I. V., Tosheva, L. & Doyle, A. M. Simultaneous removal of Cd(II), Co(II), Cu(II), Pb(II), and Zn(II) ions from aqueous solutions via adsorption on FAU-type zeolites prepared from coal fly Ash. *J. Environ. Chem. Eng.* **8**, 103895 (2020).
48. Nassar, N. N. Kinetics, equilibrium and thermodynamic studies on the adsorptive removal of nickel, cadmium and Cobalt from wastewater by superparamagnetic iron oxide nanoadsorbents. *Can. J. Chem. Eng.* **90**, 1231–1238 (2012).
49. Danila, V., Vasarevicius, S. & Valskys, V. Batch removal of Cd(II), Cu(II), Ni(II), and Pb(II) ions using stabilized zero-valent iron nanoparticles. *Energy Proced.* **147**, 214–219 (2018).
50. Lalhchingpuii, Tiwari, D., Lalmunsiamia & Lee, S. M. Chitosan templated synthesis of mesoporous silica and its application in the treatment of aqueous solutions contaminated with cadmium(II) and lead(II). *Chem. Eng. J.* **328**, 434–444 (2017).
51. Azizkhani, S., Hussain, S. A., Abdullah, N., Ismail, M. H. S. & Mohammad, A. W. Synthesis and application of functionalized graphene oxide-silica with Chitosan for removal of Cd(II) from aqueous solution. *J. Environ. Heal Sci. Eng.* **19**, 491–502 (2021).

Acknowledgements

This work was supported and funded by the Deanship of Scientific Research at Imam Mohammad Ibn Saud Islamic University (IMSIU) (grant number IMSIU-DDRSP2502).

Author contributions

Mohamed S. Kamel (Corresponding author, Methodology, Writing), Ehab A. Abdelrahman (Corresponding author, Funding acquisition, Analyses, Methodology, Writing – Review & Editing, Conceptualization), Zinab M. Anwar (Review), Samir M. El Rayes (Methodology), Mortaga M. Abou-Krishna (Visualization, Review), Raed M. Hegazey (Analyses, Conceptualization), Hanan Alhussain (Review).

Funding

This work was supported and funded by the Deanship of Scientific Research at Imam Mohammad Ibn Saud Islamic University (IMSIU) (grant number IMSIU-DDRSP2502).

Declarations

Competing interests

The authors declare no competing interests.

Consent for publication

Not applicable.

Consent to participate

Not applicable.

Ethics approval

Not applicable.

Additional information

Correspondence and requests for materials should be addressed to M.S.K. or E.A.A.

Reprints and permissions information is available at www.nature.com/reprints.

Publisher's note Springer Nature remains neutral with regard to jurisdictional claims in published maps and institutional affiliations.

Open Access This article is licensed under a Creative Commons Attribution-NonCommercial-NoDerivatives 4.0 International License, which permits any non-commercial use, sharing, distribution and reproduction in any medium or format, as long as you give appropriate credit to the original author(s) and the source, provide a link to the Creative Commons licence, and indicate if you modified the licensed material. You do not have permission under this licence to share adapted material derived from this article or parts of it. The images or other third party material in this article are included in the article's Creative Commons licence, unless indicated otherwise in a credit line to the material. If material is not included in the article's Creative Commons licence and your intended use is not permitted by statutory regulation or exceeds the permitted use, you will need to obtain permission directly from the copyright holder. To view a copy of this licence, visit <http://creativecommons.org/licenses/by-nc-nd/4.0/>.

© The Author(s) 2025